ASRL TR 1009

MEASUREMENTS OF NEAR FIELD PRESSURES OF SUBSONIC JETS

E. MOLLO-CHRISTENSEN

MASSACHUSETTS INSTITUTE OF TECHNOLOGY
AEROELASTIC AND STRUCTURES RESEARCH LABORATORY

APRIL 1963

ASRL TR 1009

UNPUBLISHED PRELIMINARY DATA

MEASUREMENTS OF NEAR FIELD PRESSURES OF SUBSONIC JETS

E. Mollo-Christensen

MASSACHUSETTS INSTITUTE OF TECHNOLOGY
AEROELASTIC AND STRUCTURES RESEARCH LABORATORY

April 1963

MEASUREMENTS OF NEAR FIELD PRESSURES OF SUBSONIC JETS

by

E. Mollo-Christensen

ABSTRACT

This paper reports on a series of measurements of pressure space-time covariance in the near field of several subsonic jets. The data include measured mean flow data, turbulence levels and power spectral densities of the pressure field outside the jet.

Among the obvious conclusions is the fact that the far field is first established for high frequencies as the distance between jet and detector are increased.

A less expected result is the long correlation distances for the larger eddies and the strong correlation across a diameter observed, both in the transitional regime and in the fully turbulent domain.

The correlation measurements show a distinction between phase velocity and group velocity of large scale disturbances.

TABLE OF CONTENTS

1. INTRODUCTION

This is one of a series of reports on experiments on free shear flows and aerodynamic noise.

The experiments, which were started in 1958 and have been supported by NASA since 1959, have been directed towards the collection of as complete and reliable information as possible involving jet flow, jet stability, turbulence and sound emission under controlled conditions.

It is our hope that the information we have, and are obtaining, may prove useful in contributing to a better and more detailed understanding of jet noise, and hopefully suggest new methods for noise prevention.

A large fraction of our effort has been devoted to making the experimental equipment work satisfactorily.

As a criterion of satisfactory operation we have used similarity in narrow band-pass spectra and other high-resolution measures. For example, we have required that power spectral density of near and far field pressure be expressible as dimensionless functions of the parameters involved. The many modifications of equipment and experimental arrangements required took approximately two years, and we obtained our first significant data in the Summer of 1961.

Among the many difficulties were scattering from microphone cables and mountings, upstream flow noise and amplifier microphonics.

At the present time, the experimental arrangement yields results which are accurate within ten per cent in root mean square for narrow band-pass spectra, and much better for mean values. The turbulence level of the flow at the jet nozzle exit is below 10^{-5}, there are no detectable

temperature or pressure fluctuations in the frequency band from 100 cycles per second to 10^5 cycles per second.

2. EXPERIMENTAL ARRANGEMENT

The experimental arrangement is shown in figure 1. Compressed dry air is supplied to a muffler-settling chamber combination, where the air passes through six steel wool pads, each four inches thick, then through a metal honeycomb, then screens of successively smaller mesh and finally into a settling chamber, from which the air enters the nozzle. The nozzles used were geometrically similar over the last four diameters of the contraction. The contraction ratio was forty for the largest nozzle (1.6 in. diameter) and four hundred for the smaller nozzle (0.5 in. diameter).

The nozzle exit is within an anechoic chamber, 8 ft x 8 ft x 8 ft, and exits through a "jet catcher" at the downstream end.

Figure 2 shows a photograph of the anechoic chamber.

3. NEAR FIELD PRESSURE MEASUREMENTS

Figure 3 shows a photograph of the microphone arrangement for near field pressure measurements. The microphones are piezoelectric microphones with a sensitive area of 1.5 mm diameter and a frontal diameter of 3 mm.

Figure 4 shows a block diagram of the data processing system. We decided upon "on-the-line" data processing as preferable to recording and later playback for data processing. One advantage is that reasons for suspicious data can be investigated immediately.

The signals are fed to a tape recorder and played back at a variable delay. The delayed signals are multi-

plied together, integrated with respect to time and recorded versus delay time.

Figure 5 shows the time delay arrangement with delay time drive.

Figure 6 demonstrates the performance of the correlator. The microphone was placed one diameter downstream of the nozzle exit plane, a small distance away from the jet. The dotted line shows the autocorrelation for jet exit Mach number 0.48. The time scale was obtained by autocorrelating a 20 kc signal; this correlation is shown as a dotted line in the lower part of the figure.

The zero time delay point was obtained by recording the autocorrelation of white noise from a white noise generator. Next, the time scale was expanded by changing the sensitivity of the x-y recorder. The time scale was established as expanded by a factor of two by recording the autocorrelation of a 20 kc signal, the solid line in the lower part of the diagram. Finally, the pressure autocorrelation was recorded at a jet Mach number of 0.96, and the solid line autocorrelation obtained.

The reason for the apparent shift in the maximum of the correlation function is that two colors of ink, and therefore two different recording pens, were used. It was found that one recording pen was 0.10 inches longer than the other; this explains most of the discrepancy.

3.1 Coordinate System, Notation

Figure 7 shows the coordinate system used in the near field.

x	is the distance from the nozzle exit plane
r	is the distance from the nozzle lip
θ	is the angle between r and the jet axis
D	is the jet diameter

Adopt the following notation:

p	pressure fluctuation
t	time
Δx	microphone displacement
τ	time displacement
U	jet exit velocity
M	jet exit Mach number
ω	frequency, radians per second
$(\tilde{})$	superscript, root mean square
$< >$	time averaged

$$C_{pp}(x, \Delta x, \tau) = \frac{\langle p(x,t)\ p(x + \Delta x,\ t + \tau)\rangle}{\tilde{p}(x)\ \tilde{p}(x + \Delta x)}$$, the pressure correlation coefficient.

$$\Phi(\omega) = 4 \int_0^\infty \langle p(x,\ t)\ p(x,\ t + \tau)\rangle \cos \omega\tau\ d\tau$$, the power spectral density (here measured directly).

3.2 Variation of Root-Mean-Square Pressure along Jet

Figure 8 shows a typical variation of $\tilde{p}(x,\theta)$ for constant θ for one jet Mach number.

Figure 9 shows the variation of $\tilde{p}(x,\theta)$ ror constant distance 3D/2 from the jet axis. The data indicate that there is a change in the variation of $\tilde{p}$ with Mach number near M = 0.3. Other indications of this will be shown later.

Figure 10 shows some correlation functions across the jet diameter for $\theta = 20^{\circ}$, $x/D = 4$ and 6, and for three Mach numbers. Plotted are the autocorrelations of the two microphone signals and their cross correlation versus delay time. The autocorrelations should be identical under perfect conditions. The lack of perfection is partly due to slightly different sensitivity settings, while there also appears, in the upper right-hand figure, a slight indication of microphone vibration.

The information obtained from a large number of such measurements are shown in the next two figures.

3.3 Correlation Across a Jet Diameter

Figure 11 shows the cross-correlation coefficient at zero time delay across a diameter for several values of M and x/D, for one jet diameter, namely D = 1/2 in.

It is remarkable how the variation of correlation coefficient changes when M becomes larger than 0.3.

Figure 12 shows the correlation coefficient for points 90° apart around the jet circumference, for different Mach numbers, distances from the nozzle exit and for two different nozzle diameters, namely D = 1/2 in. and D = 1 in. The points from the two nozzles coincide. Again, something seems to happen near M = 0.3.

3.4 Power Spectral Densities of Pressure Fluctuations in the Near Field

The power spectral densities were measured with a power bandwidth of 45 cps over the frequency range of 200 cps to 50,000 cps.

Figure 13 shows the square root of power spectral

$\sqrt{\Phi(\omega)}$ plotted versus Strouhal number based on streamwise location $\omega x/2\pi U$, and at exit Mach number of 0.6. The similarity at large frequencies is apparent. A similar set of spectra for M = 0.9 is shown in figure 14.

If, perhaps against expectations, far field similarity should be established anywhere, i.e., that $\sqrt{\Phi(\omega)}/r$ is a constant, and if $\Phi(\omega D/U) \sim (\omega D/U)^n$, one should expect $\Phi(\omega x/U)$ to coalesce. This is the case for the high frequencies in figures 13 and 14.

The high frequency portion of the spectrum is most likely to have been emitted from the upstream portion of the jet. Another explanation is of course that the turbulent wave numbers just scale with 1/x. The choice of explanation is not obvious.

Figures 15, 16, 17 and 18 show a set of pressure spectra for jet Mach number 0.90. Figure 14 was obtained by cross-plotting samples of these spectra. Figures 19 and 20 show how the high frequency portion of the spectra approach far field similarity quite near the jet.

3.5 Space-Time Correlations of Pressure in the Near Field Just Outside the Jet

Figure 21 shows pressure correlation coefficient

$$C_{pp}(x, \Delta x, \theta, \tau) = \frac{\langle p(x,\theta,t)\ p(x+\Delta x, \theta, t+\tau)\rangle}{\tilde{p}(x,\theta)\ \tilde{p}(x+\Delta x, \theta)}$$

for two Mach numbers, plotted versus $U\tau/D$ for four values of Δx.

The distance from the nozzle exit plane to the upstream microphone was x = D. The jet diameter D was one inch. The similarity is remarkable.

An alternative way of plotting the data from figure 21 is shown in figure 22, where contours of constant correlation coefficient are shown. Two lines of constant correlation velocity $\Delta x/\tau$ have been drawn.

It appears that the correlation velocity is between U/2 and U, and much closer to the latter for this particular case. In order to examine this in more detail, we include a number of correlation curves, as shown in figures 23 to figure 33, inclusive.

Figure 23 shows the pressure autocorrelations for $x/D = 1/2$; $M = 0.15$; $D = 1/2$ in.; the jet is laminar and the microphone is upstream of the unstable part of the shear layer. The autocorrelation for $x/D = 1$ shows the pressure fluctuations associated with the Tollmien-Schlichting waves of the free shear layer.

Examining the cross correlation one finds that the fluctuations of the frequency of the Tollmien-Schlichting waves are correlated for $\Delta x/D = 0.5$ and 1, but that for $\Delta x/D = 2$, a lower frequency seems to dominate the cross correlation. The correlation phase velocity appears to be approximately U/3; which indicates a significant standing wave part in the instability fluctuations.

Figure 24 shows how the correlation function persists with increasing separation Δx for $M = 0.3$, the distance required for the correlations coefficient to decrease by a factor of $1/e$ being approximately 1.5D when $x/D = 1/4$. This decrement distance remains about the same for $x/D = 1/2$ as shown in figure 25, while figure 26 shows it to be increased significantly for $x/D = 1$. At the same time, the correlation speed increases with increasing x/D, from U/2 at $x/D = 1/2$ to somewhere near 0.7U at $x/D = 1$. At $M = 0.6$, as shown in

figures 27, 28 and 29, the correlation speed seems to have increased to 0.7U at x/D = 1/4, and to almost U at x/D = 1, while the persistence of the correlation coefficient with increasing x/D is very noticeable.

Figure 30 again shows that the correlation speed is larger than U/2 for x/D = 1/4 for M = 0.8.

Figures 31, 32 and 33 show that the correlation speed again increases with increasing Mach number and with x/D while the persistence of the correlation coefficient increases with increasing x/D.

Figure 34 shows a first crude estimate of the variation of correlation speed with Mach number and x/D.

3.6 Approximate Form of the Correlation Function

Among the many features of the pressure correlation coefficient in a streamwise direction, the following are worth mentioning.

The autocorrelation is of course symmetric about $\tau = 0$. The cross correlation becomes antisymmetric about a certain τ for some finite value of Δx, then it becomes symmetric about some other τ at slightly larger Δx, and so forth.

It is as if the correlation function were composed of

(a) A simply harmonic wave travelling at a speed V_1 with respect to the microphone $\cos k(\Delta x - V_1\tau)$ multiplied by

(b) A weighting function looking somewhat like a Gaussian curve travelling at a speed V_2:

$$\exp\left\{(\Delta x - V_2\tau)^2/\sigma^2\right\}$$

multiplied by

(c) An exponential decay

$$e^{-\frac{\Delta x}{\ell x}}$$

where $\ell \cdot x$ is a decay distance.

A reasonable first approximation to the form of the correlation function is therefore

$$C_{pp}(x, \Delta x, \tau) = \exp\left\{ \frac{-\Delta x}{\ell x} - [(\Delta x - V_2\tau)/\sigma]^2 \right\} \times \cos \frac{\omega U}{D} \left(\frac{\Delta x - V_1 \tau}{x}\right) \quad (1)$$

where V_1 and V_2 are correlation "group" and "phase" velocities, respectively.

By differentiating Eq. 1 with respect to the various parameters one can generate other correlation functions and obtain a complete set of functions of Δx on the infinite interval. Linear superposition can then be used to attain closer approximation than is possible with a single term as in Eq. 1.

This is hardly worthwhile before one either knows or understands the actual physical processes in much more detail and to a higher precision than is the case at the present.

4. THE PRINCIPAL OBSERVED FEATURES OF THE NEAR PRESSURE FIELD

The pressure field near the jet appears to be much more coherent than was believed previously. This may in some measure be due to the extreme precautions taken in our experiments to avoid parasitic influences. Our experiments therefore probably do not agree with crude experi-

ments on small laboratory scale. One may find that they agree better with full-scale experiments, where the parasitic influences probably are of smaller relative scale than in the laboratory. This has not been checked. Full-scale experimental results, where neither the jet nor the microphone was near a solid boundary, are not readily available.

The streamwise variation of the correlation of pressure across a diameter and around the jet circumference indicates that Mach number is an important parameter in the processes of generation of turbulence in the jet.

The increase in correlation velocity of streamwise correlations of pressure indicates that part of what was observed was sound travelling downstream in the jet. The fact that there was an observable difference between correlation phase velocity and correlation group velocity indicates that one most likely is observing a phenomenon related to hydrodynamic instability. Such an instability would tend to grow or decay in group length of a disturbance train at a different rate on the upstream and downstream ends of the group. The correlation resulting from a random train of such disturbance packages would give different phase and group velocities.

That there exists a strong possibility that coupling exists between the sound travelling inside the jet and the instability fluctuations or mechanism of generation of turbulence is obvious from an examination of the equations of motion. This will be shown in the next section.

The correlation measurements also indicate that the longer streamwise and lateral correlations which exhibit the features just discussed are the low frequency part of the disturbances, since the correlation functions do not have

as sharp maxima as do the autocorrelations. This is to be expected, namely that the larger eddies persist longer in distance and time than the small ones. A comforting but obvious result.

5. INTERACTION BETWEEN CONVECTED SOUND AND VORTICITY FLUCTUATIONS IN THE PRESENCE OF MEAN SHEAR

Describe the velocity field $\vec{u}(\vec{x},t)$ as a sum of three velocity fields,

$$\vec{u}(\vec{x},t) = \vec{U}(\vec{x}) + \vec{v}(\vec{x},t) + \vec{w}(\vec{x},t), \text{ where}$$

$\vec{U}(\vec{x})$ the local time average velocity

$\vec{v}(\vec{x},t) = \nabla\varphi(\vec{x},t)$ the irrotational part of the fluctuating field

$w(\vec{x},t) = \text{curl}\,\vec{\psi}(\vec{x},t)$ the solenoidal part of the fluctuating field.

Without loss of generality, one may set $\text{div}\,\vec{\psi} = 0$.

The equation of continuity relates the potential field directly to density fluctuations:

$$\left\{ \frac{D}{Dt} \left(\ell n \frac{\rho}{\rho_o} \right) \right\}' + \nabla^2\varphi = 0 \qquad (2)$$

where the prime $\{\ \}'$ denotes the time dependent part of a quantity. D/Dt is the total derivative, including the convection by velocity fluctuations.

The momentum equation is

$$\rho \frac{D\vec{u}}{Dt} + \text{grad}\ p = \text{div}\ \mathcal{T} \qquad (3)$$

$\mathcal{T}$ being the viscous stress tensor.

The energy equation is

$$\rho T \frac{DS}{Dt} = \Phi + \text{div } (k \text{ grad } T) \tag{4}$$

The equations of state are written as

$$p = \rho R T \tag{5}$$

$$a^2 = \gamma \frac{p}{\rho}$$

$$\frac{dp}{\rho} = a^2 \frac{d\rho}{\rho} + (\gamma - 1) T \, dS \tag{6}$$

p, ρ, T, a^2 and S being state variables, any two being sufficient to describe the state of the gas.

Taking the curl of the momentum equation and performing a number of operations using the other equations, one finds a form of the equation for the transport of vorticity, namely:

$$\begin{aligned}
&- \left(\frac{\partial}{\partial t} + \vec{U} \cdot \nabla\right) \nabla^2 \vec{\psi} + (\text{curl } \vec{\psi} \cdot \nabla) \text{ curl } \vec{U} \\
&+ (\text{curl } \vec{U} \cdot \nabla) \text{ curl } \vec{\psi} + \nabla^2 \vec{\psi} \text{ div } \vec{U} \\
&+ (\nabla\varphi \cdot \nabla) \text{ curl } \vec{U} + (\text{curl } \vec{U} \cdot \nabla) \nabla\varphi - \text{curl } \vec{U} \nabla^2\varphi \\
&+ \Big\{ - [(\nabla\varphi + \text{curl } \vec{\psi}) \cdot \nabla] \nabla^2 \vec{\psi} - (\nabla^2 \vec{\psi} \cdot \nabla)(\nabla\varphi + \text{curl } \vec{\psi}) \\
&+ \nabla^2 \varphi \, \nabla^2 \vec{\psi} \Big\}' = \\
&= - \left\{ \text{curl } \left(\frac{\text{div } \mathcal{T}}{\rho} \right) \right\}' - \left\{ \nabla T \times \left[\gamma R \, \ell n \frac{\rho}{\rho_o} + (\gamma - 1) \nabla S \right] \right\}'
\end{aligned} \tag{7}$$

There is, therefore, a linear as well as a nonlinear coupling between vorticity fluctuations and density fluctuations. For an unstable mean flow, a small density disturbance may cause a large vorticity disturbance, if the density disturbance is just right or near the conditions for linear

resonance. The occurrence of such density disturbances is not unlikely, since vorticity fluctuations will generate density fluctuations, as has been shown by Lighthill.

This is a possible explanation of the strongly coherent low frequency near field pressure patterns. Of course, correlation measures only the coherent part, which may be a small fraction of the total energy in the fluctuating field.

On the other hand, a coherent emitter is much more efficient than a random emitter. Even if it is weak, it may emit more than a much more intense random emitter.

Also, we should remember that incoherence and coherence are distinctions of degree, rather than kind when one thinks about spatially extensive emitters, and that one may think in terms of degrees of coherence.

6. FAR FIELD MEASUREMENTS

Our far field measurements show that the low-frequency maximum of the far field power spectral density is sensitive and depends strongly upon whether transition occurs in the free shear layer of the jet or in the nozzle. This also affects the rms pressure fluctuations in the near field, and thus the magnitude of the correlation function in the near field, as contrasted to the correlation coefficient.

Figure 35 shows a number of far field spectra, and illustrates the dependence upon the low frequency peak of far field power spectrum upon jet diameter. The detailed results of our far field measurements has been printed as a separate report, and is being submitted for publication.

7. SUGGESTIONS FOR FURTHER WORK

We are currently investigating the effect of changes in the mean flow upon the near field streamwise pressure correlations. We have observed effects, and are pursuing the investigations further.

A promising avenue for further work may be to attempt to make the noise field different from axisymmetric.

It may be possible to do this by mean flow modifications. Even if the total noise from a jet engine would then be increased, if most of the noise would be directed upwards, for example, it would perhaps be less bothersome on the ground.

In such work, I would like to emphasize the need for careful and controlled experiments. We may have gone too far in this respect, a criticism of our work being that real jets are not all that pure, and that our work therefore is not clearly applicable to practical circumstances.

Even if this is so, we have the comfort to know what we have been measuring, and we find it an interesting area of fluid dynamics, of ultimate use beyond jet noise prevention.

8. ACKNOWLEDGMENT

This work was supported by the National Aeronautics and Space Administration under Grant NsG 31-60.

The author wishes to acknowledge the contributions of Mr. F. Merlis, whose efforts made the experimental work possible.

BIBLIOGRAPHY

1. Lighthill, M.J. On Sound Generated Aerodynamically - Part I - General Theory, Proceedings, Roy. Soc. A, Vol. 211, pp. 564-587, 1952.

2. Lighthill, M.J. On Sound Generated Aerodynamically - Part II - Turbulence as a Source of Sound, Proceedings, Roy. Soc. A, Vol. 222, pp. 1-32, 1954.

3. Lighthill, M.J. Sound Generated Aerodynamically, The Bakerian Lecture, 1961, published by Royal Aircraft Establishment, as Report Dir. 8 (November 1961).

4. Ribner, H.S. Aerodynamic Sound from Fluid Dilatations - A Theory of the Sound from Jets and Other Flows, Institute of Physics, University of Toronto, July 1962, UTIA Rept. No. 86 (AFOSR TN 3430).

5. Williams, J.E. Ff. "Noise from Convected Turbulence" 62nd Meeting, Acous. Society of America, Cincinnati, November 8-11, 1961.

6. Corrsin, S. Investigation of Flow in an Axially Symmetrical Heated Jet of Air, NACA Wartime Report No. W. 94 (ACR 3123).

7. Corrsin, S. and Kistler, A.L. Free Stream Boundaries of Turbulent Flows, NACA Report 1244.

8. Corrsin, S. and Uberoi, M. Further Experiments on the Flow and Heat Transfer in a Heated Turbulent Air-Jet, NACA TN No. 1865.

9. Corrsin, S. and Uberoi, M. Spectra and Diffusion in a Round Turbulent Jet, NACA Report No. 1040.

10. Grane, L.J. and Pack, D.C. The Laminar and Turbulent Mixing of Jets of Compressible Fluid, Part I - Flow Far from the Orifice, Journal of Fluid Mechanics Vol. 2, No. 5, pp. 449-455, 1957.

11. Kanpur, J.N. Transverse Component of Velocity in a Plane Symmetrical Jet of a Compressible Fluid, Quarterly Journal Mech. Applied Mathematics, Vol. II, No. 4, pp. 423-426, November 1958.

12. Laurence, J.C. Intensity, Scale and Spectra of Turbulence in Mixing of Free Subsonic Jet, NACA Tech. Report 1292, April 1956.

13. Lassiter, L.W. Turbulence in Small Jets at Exit Velocities up to 705 ft/sec, Journal of Applied Mechanics, Vol. 24, pp. 349-354, September 1957.

14. Liepmann, H.W. and Laufer, J. Investigation of Free Turbulent Mixing, NACA TN 1257, 1947.

15. Morkovin, Mark V. Note on Turbulence in Small Air-Jets at Exit Velocities up to 705 Feet Per Second, Journal of Applied Mechanics, Vol. 25, June 1958.

16. Kolpin, M.A. Flow in the Mixing Region of a Jet. National Aeronautics and Space Administration Grant NsG-31-60, ASRL TR 92-3, June 1962.

17. Mollo-Christensen, E. Jet Flow and Jet Noise, MIT ASRL TR 1006, January 1963.

18. Mollo-Christensen, E., Kolpin, M.A., Martuccelli, J.R., Experiments on jet flow and jet noise - far field spectra and directivity patterns. MIT ASRL 1007, February 1963.

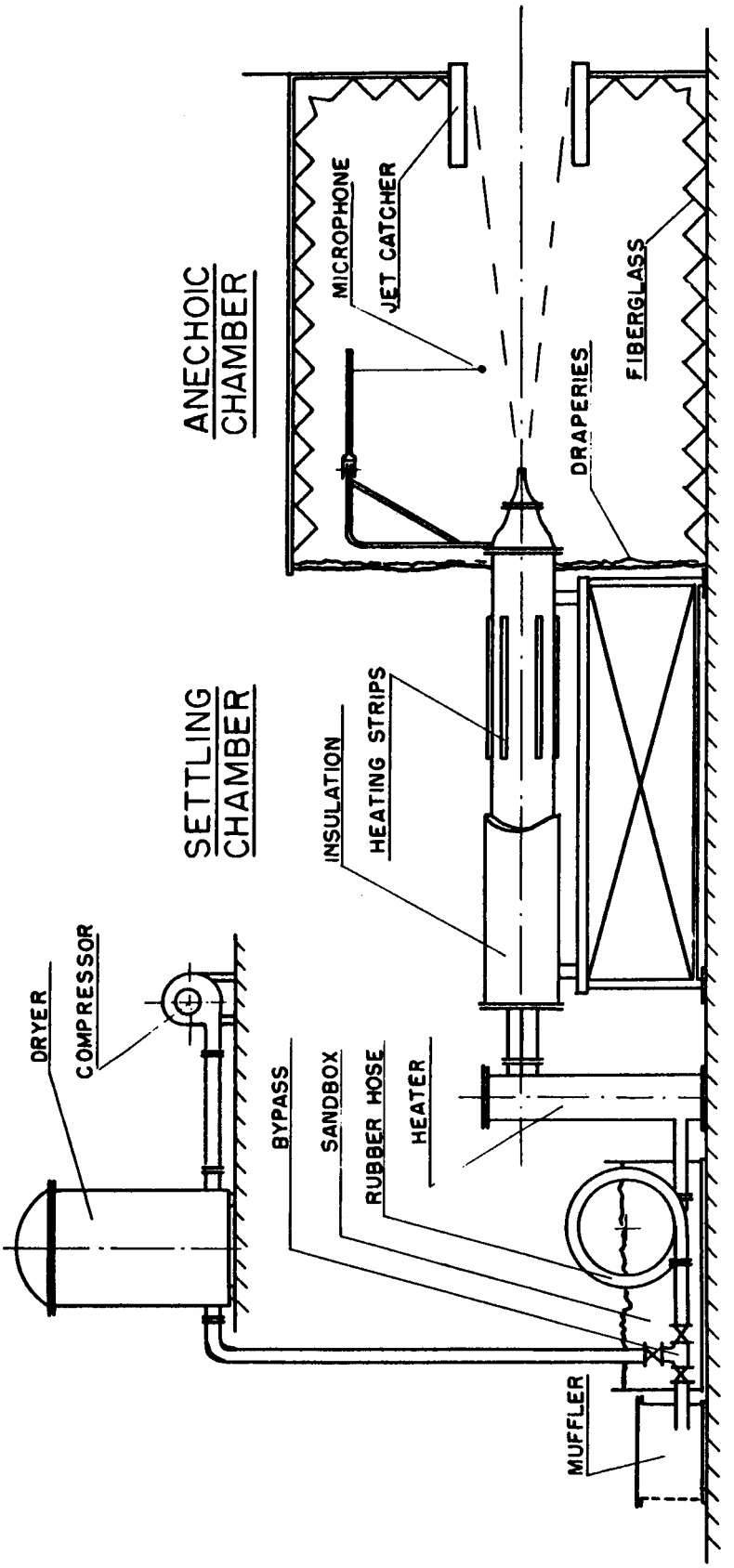

Figure 1 Flow Apparatus

Figure 2 Anechoic Chamber

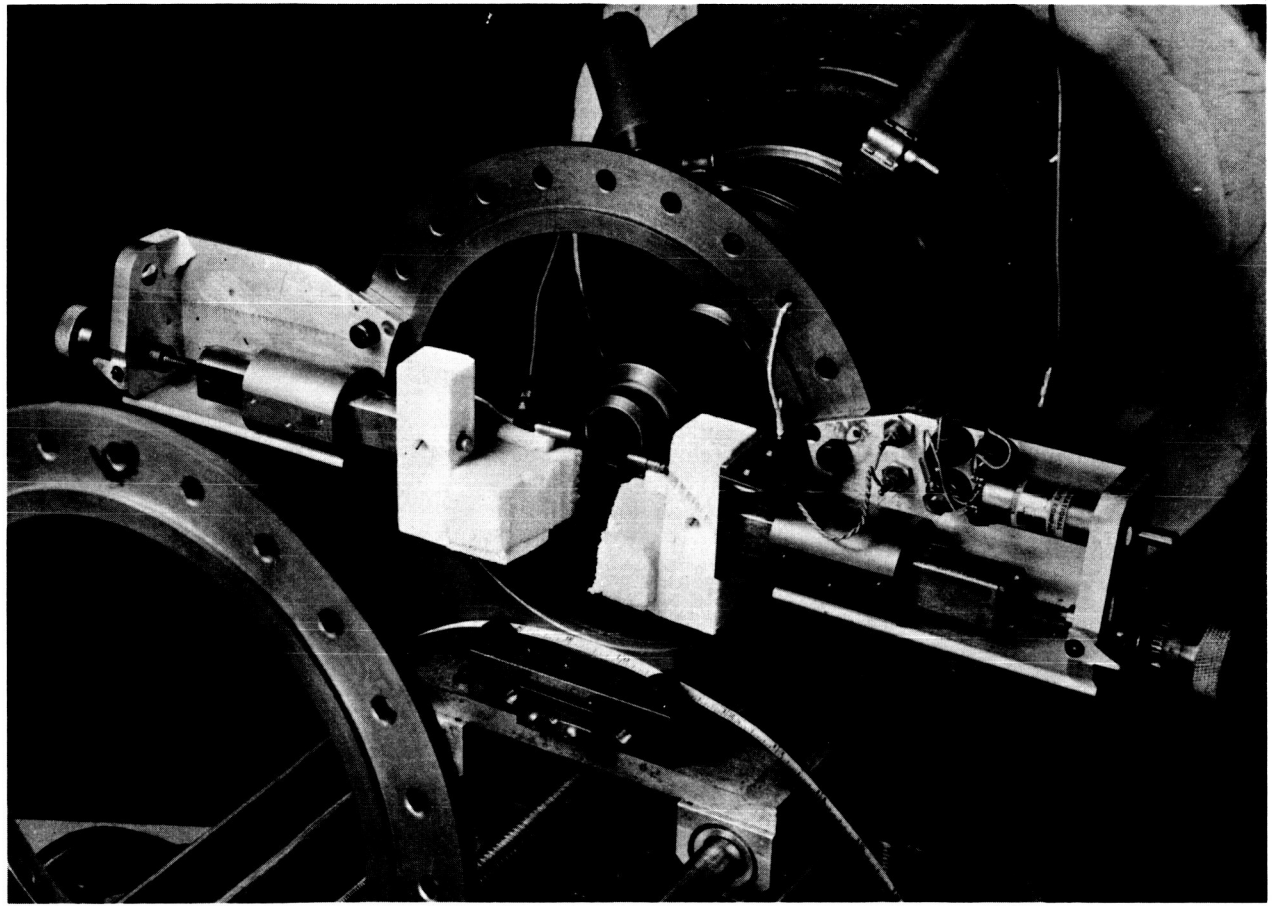

Figure 3 Microphone Arrangement for Near Field Pressure Measurements

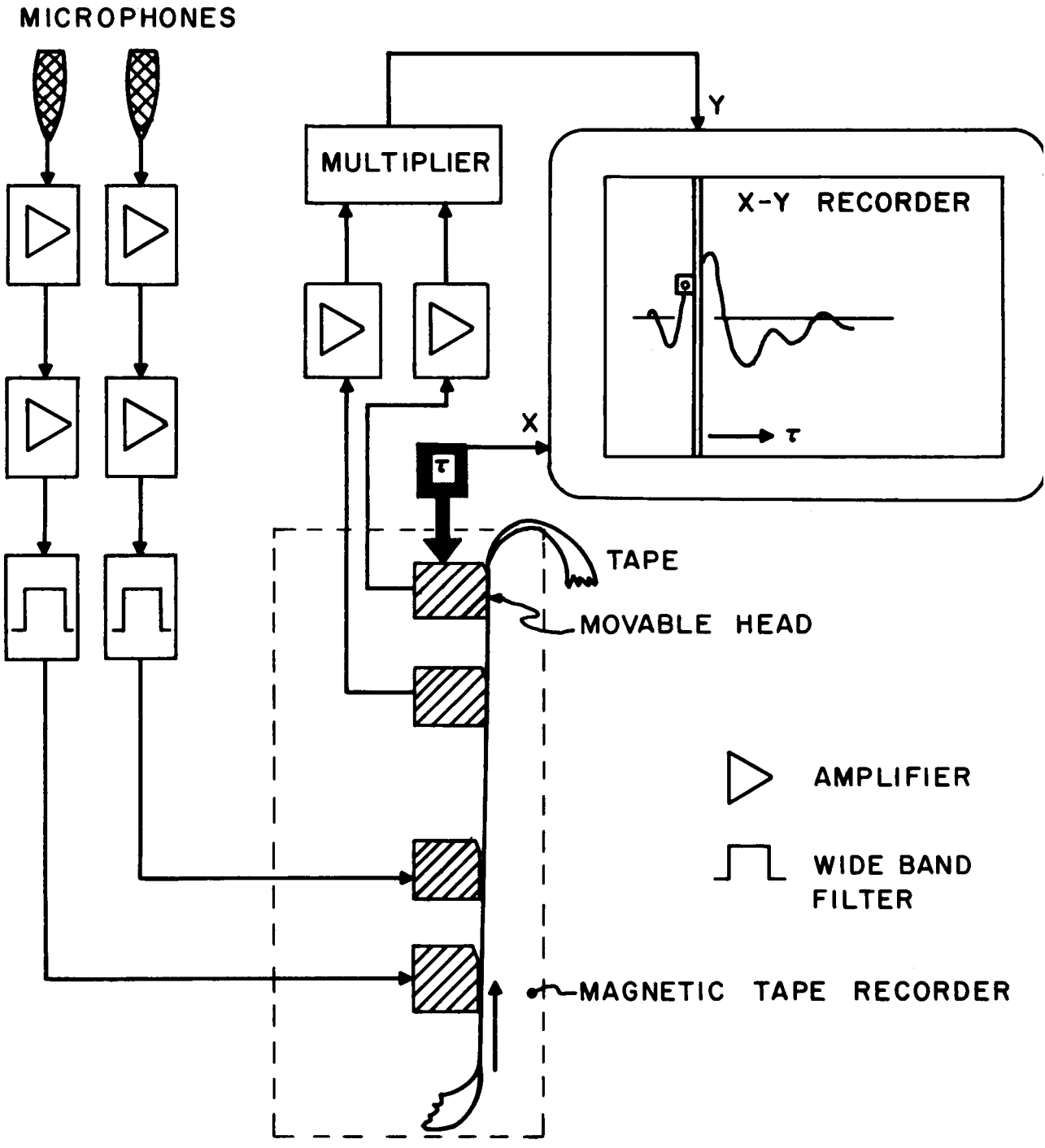

Figure 4 Block Diagram

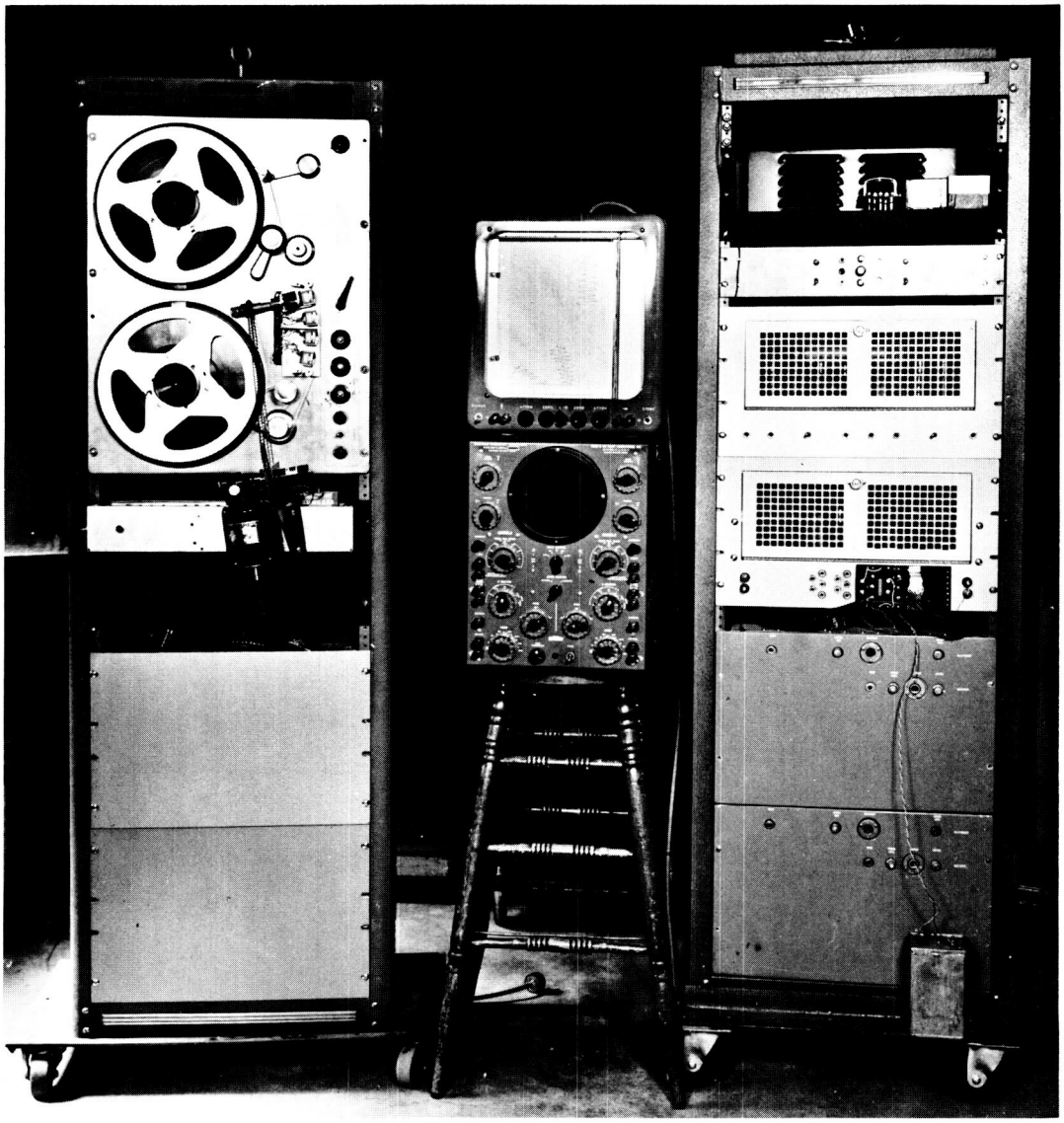

Figure 5. Photo of Analysis Equipment

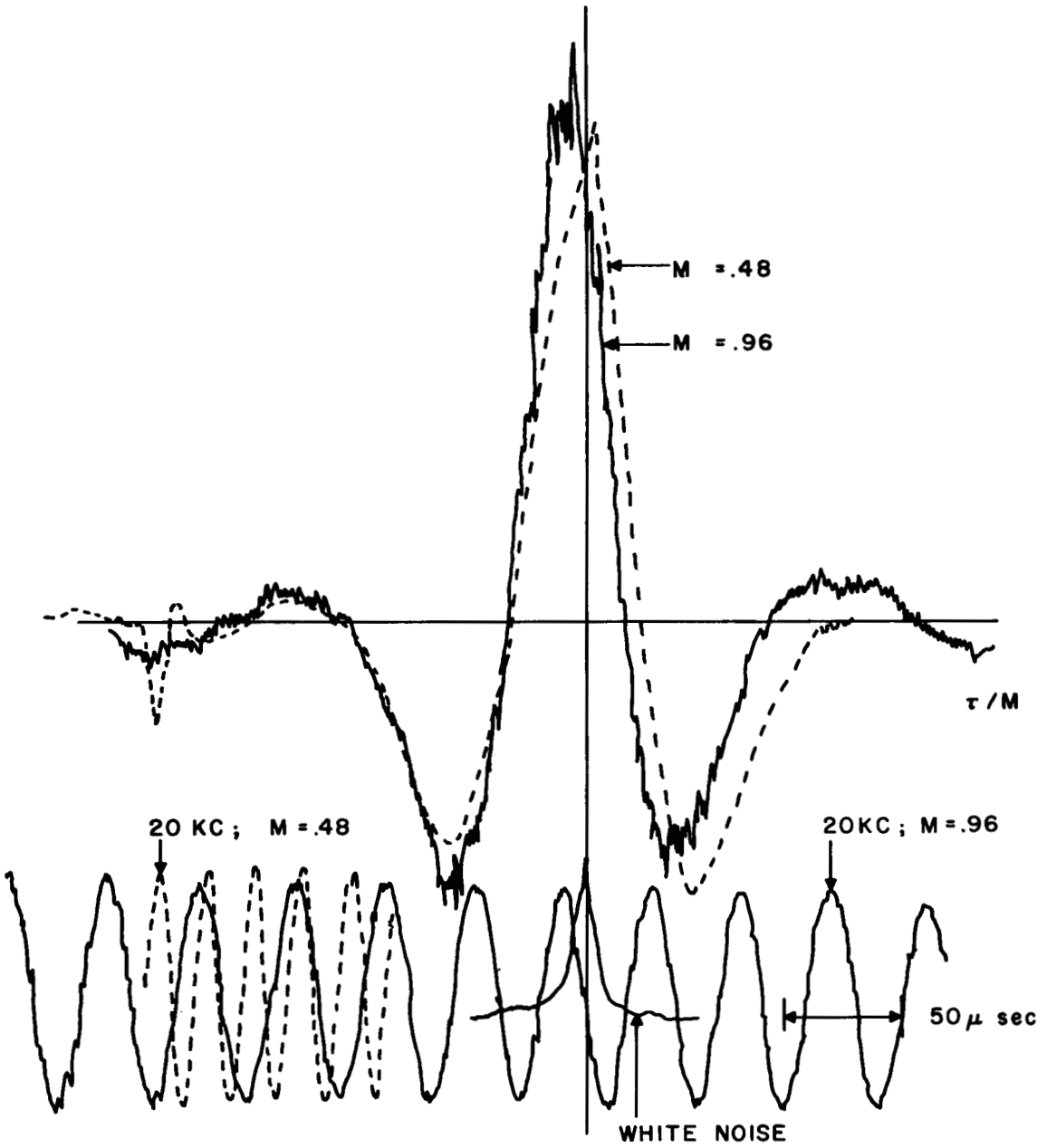

Figure 6. Similarity in Near Field Pressure Correlations

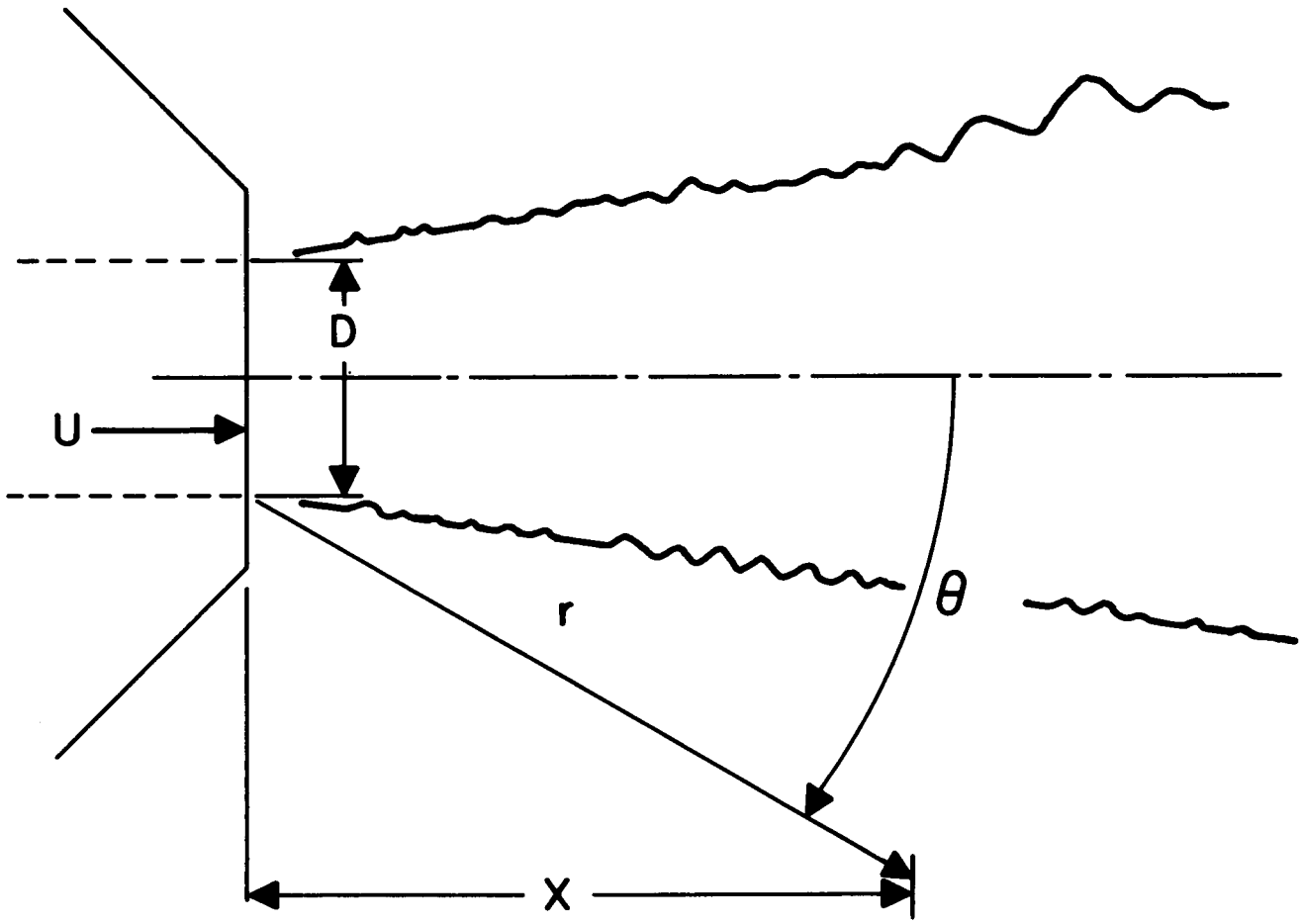

Figure 7. Coordinate System

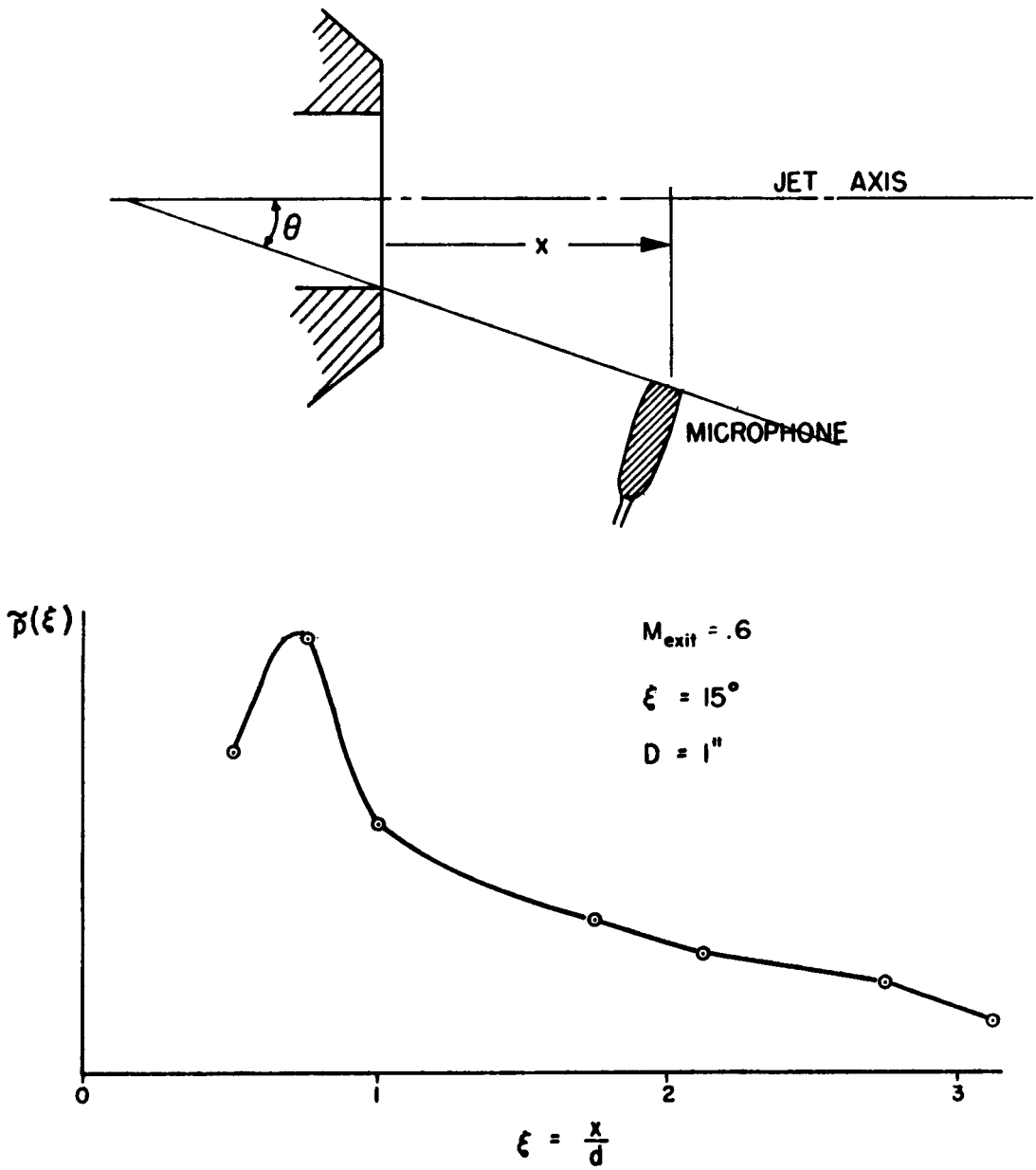

Figure 8. Variation of RMS Pressure Fluctuation with Distance Along the Jet

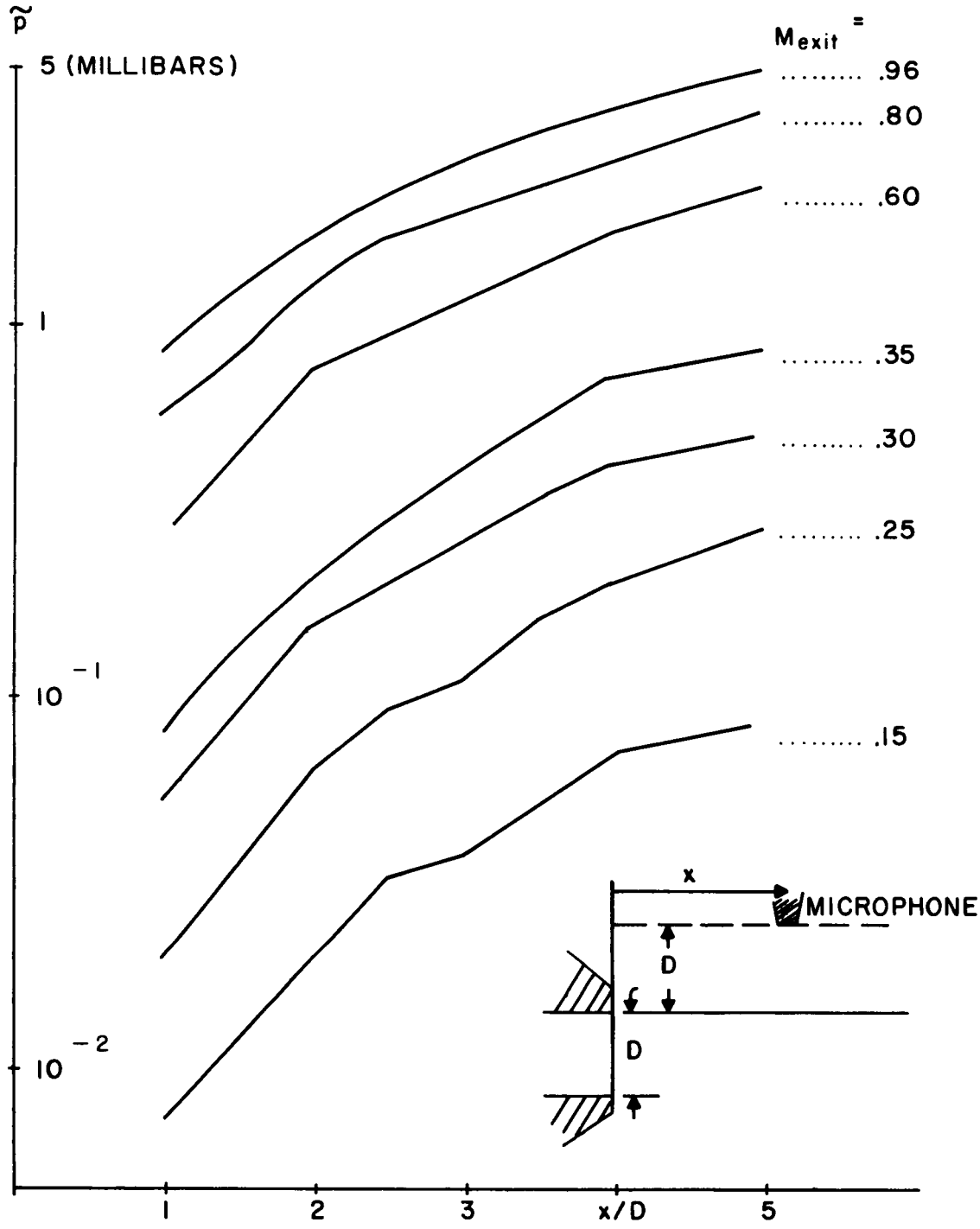

Figure 9. RMS Pressure Fluctuations as Function of x/D for Different Exit Mach Numbers, D = 1 in.

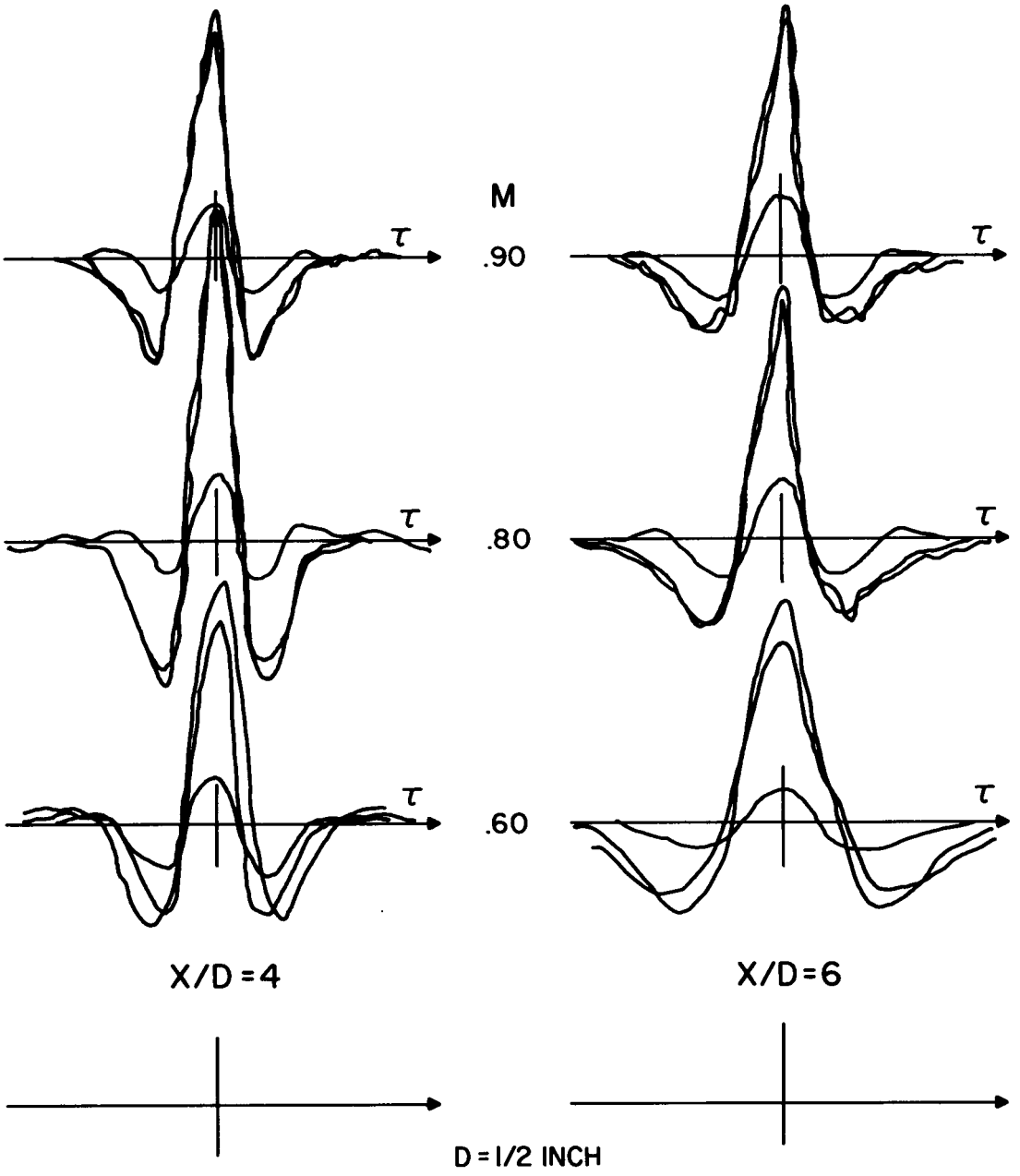

Figure 10. Pressure Autocorrelations on Opposite Sides of the Jet and Cross Correlations for Different Values of x/D and M.

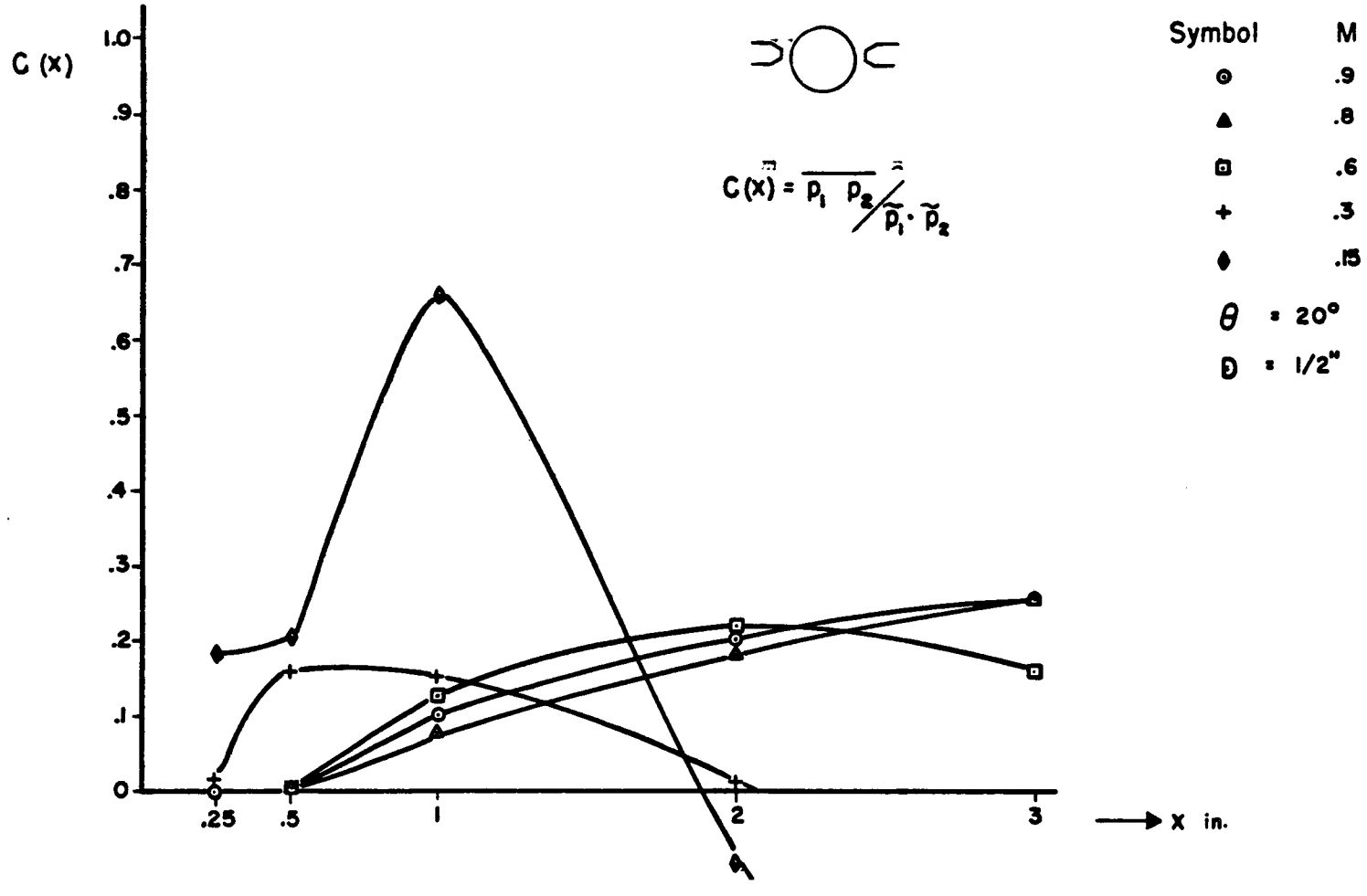

Figure 11. Cross Correlation Across a Jet Diameter

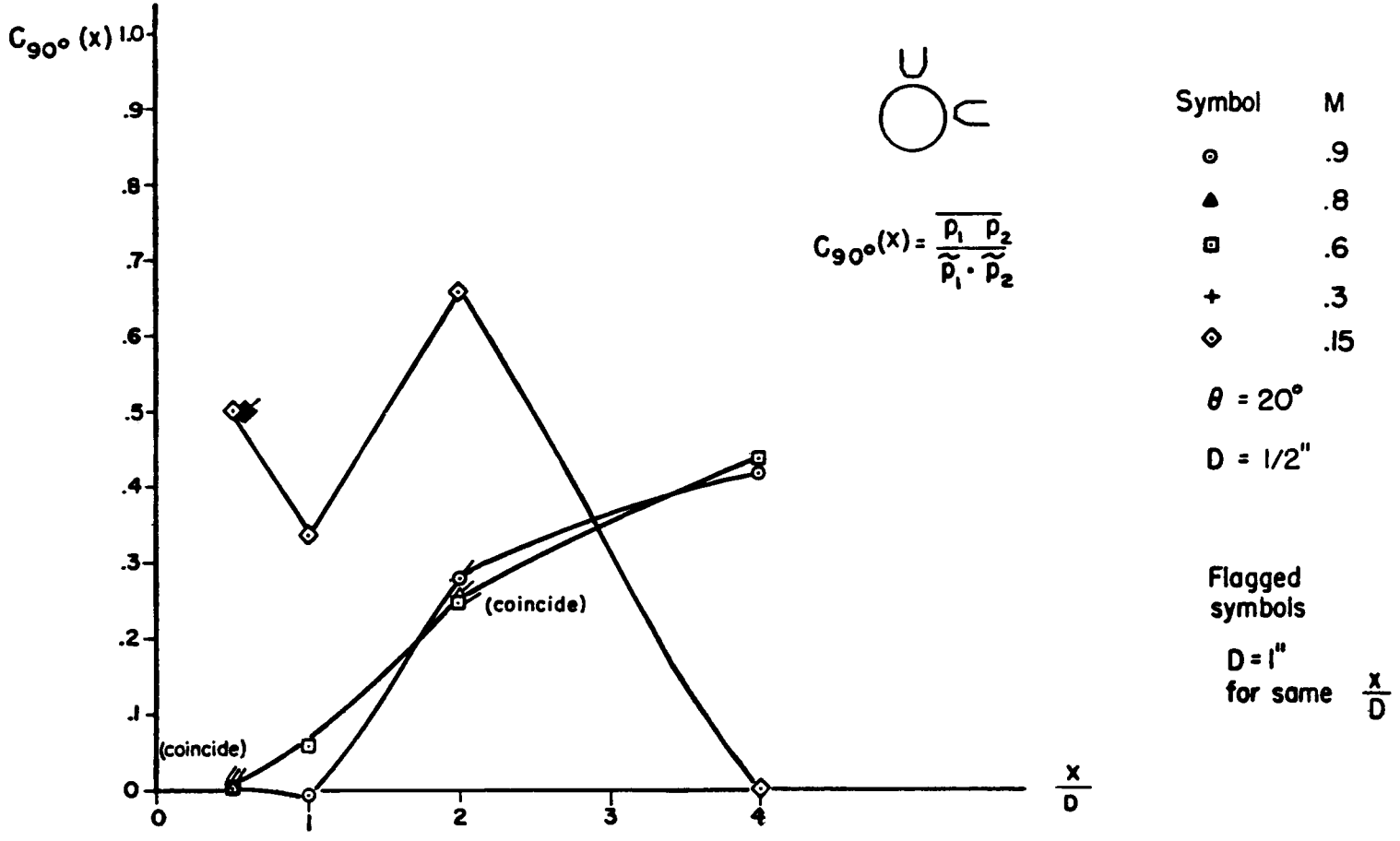

Figure 12. Cross Correlation between Points Separated by 90° around the jet circumference

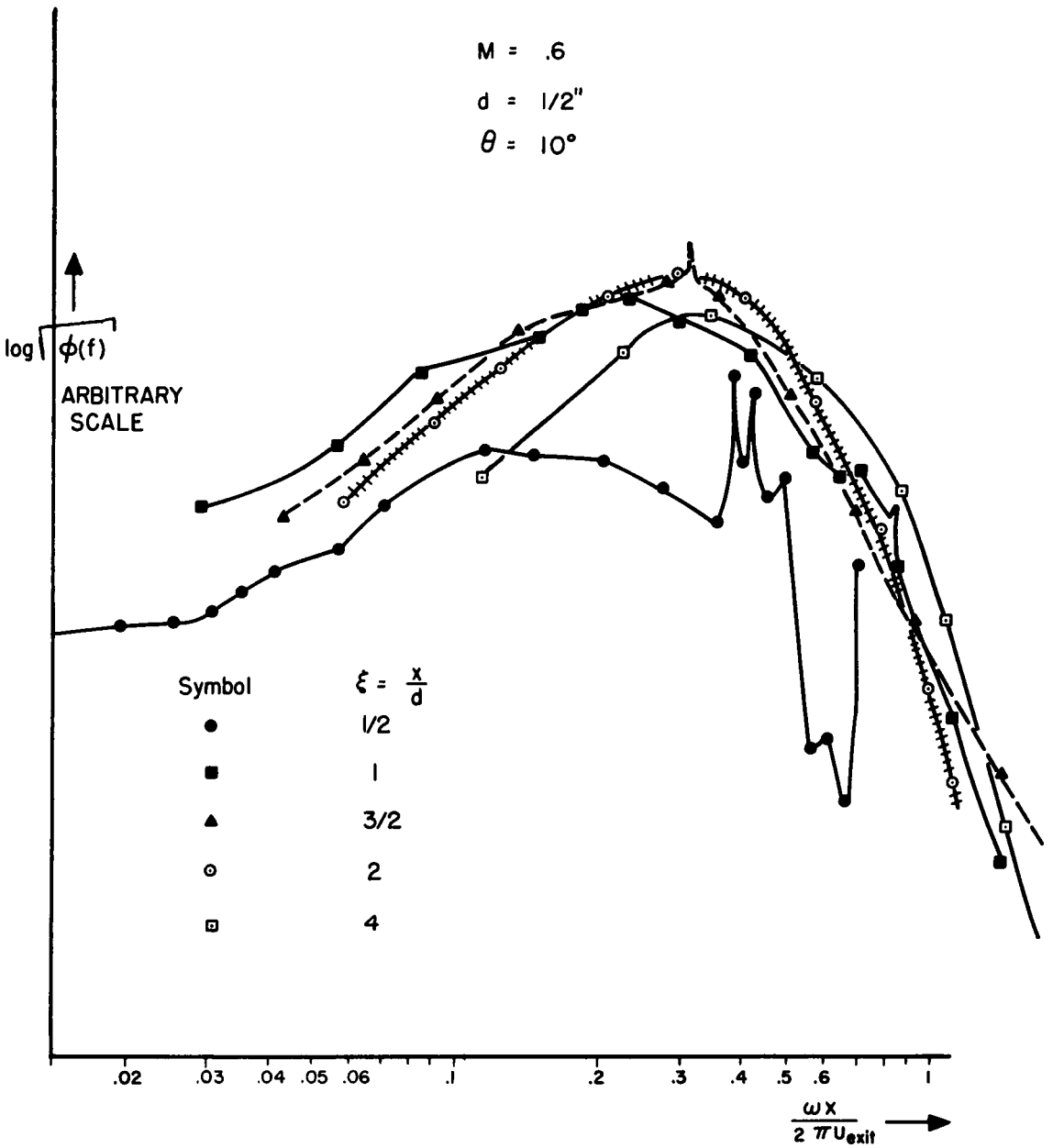

Figure 13. Near Field Pressure Spectra at Several Streamwise Locations.

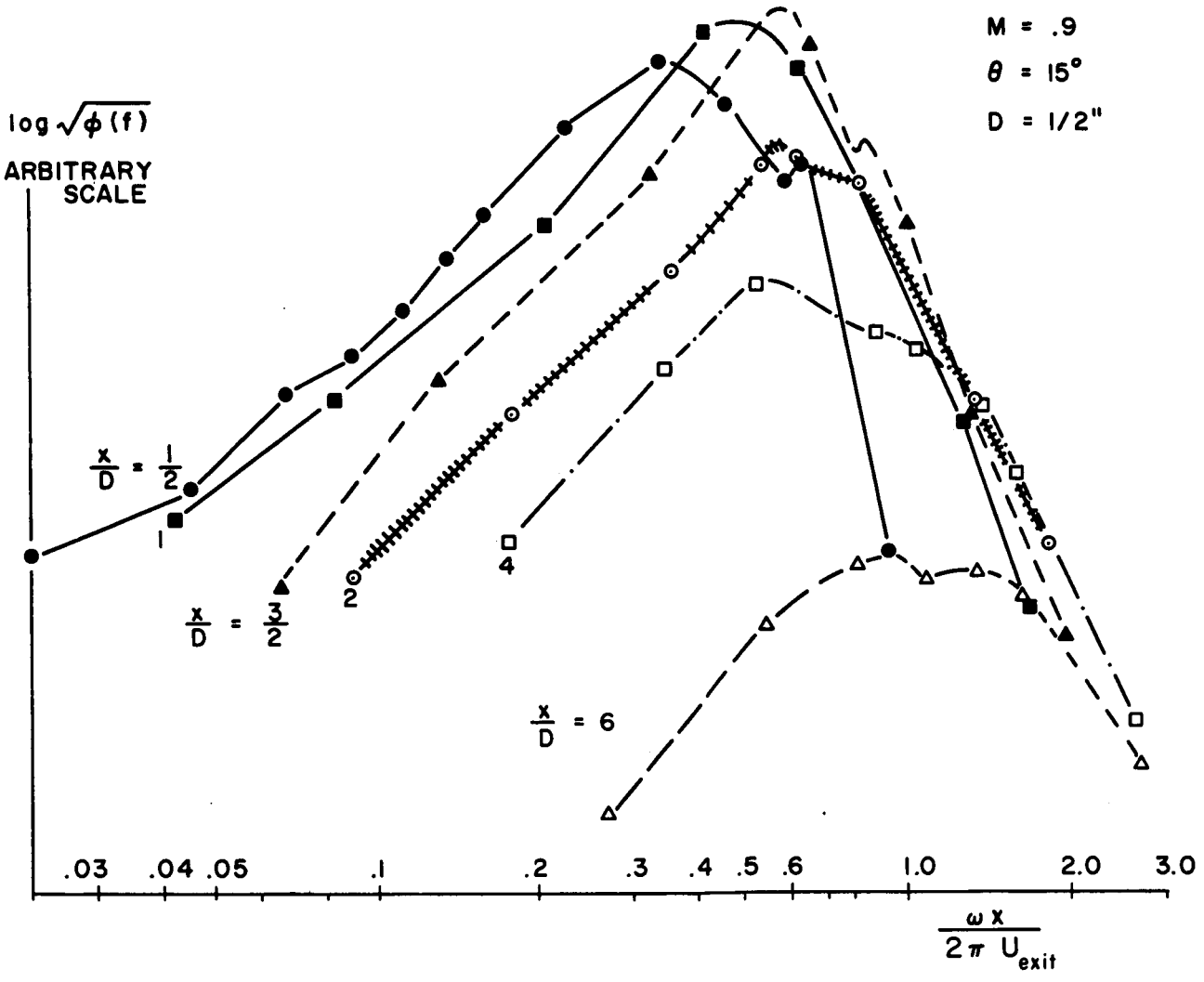

Figure 14. Near Field Spectra $\theta = 15^{\circ}$, M = 9

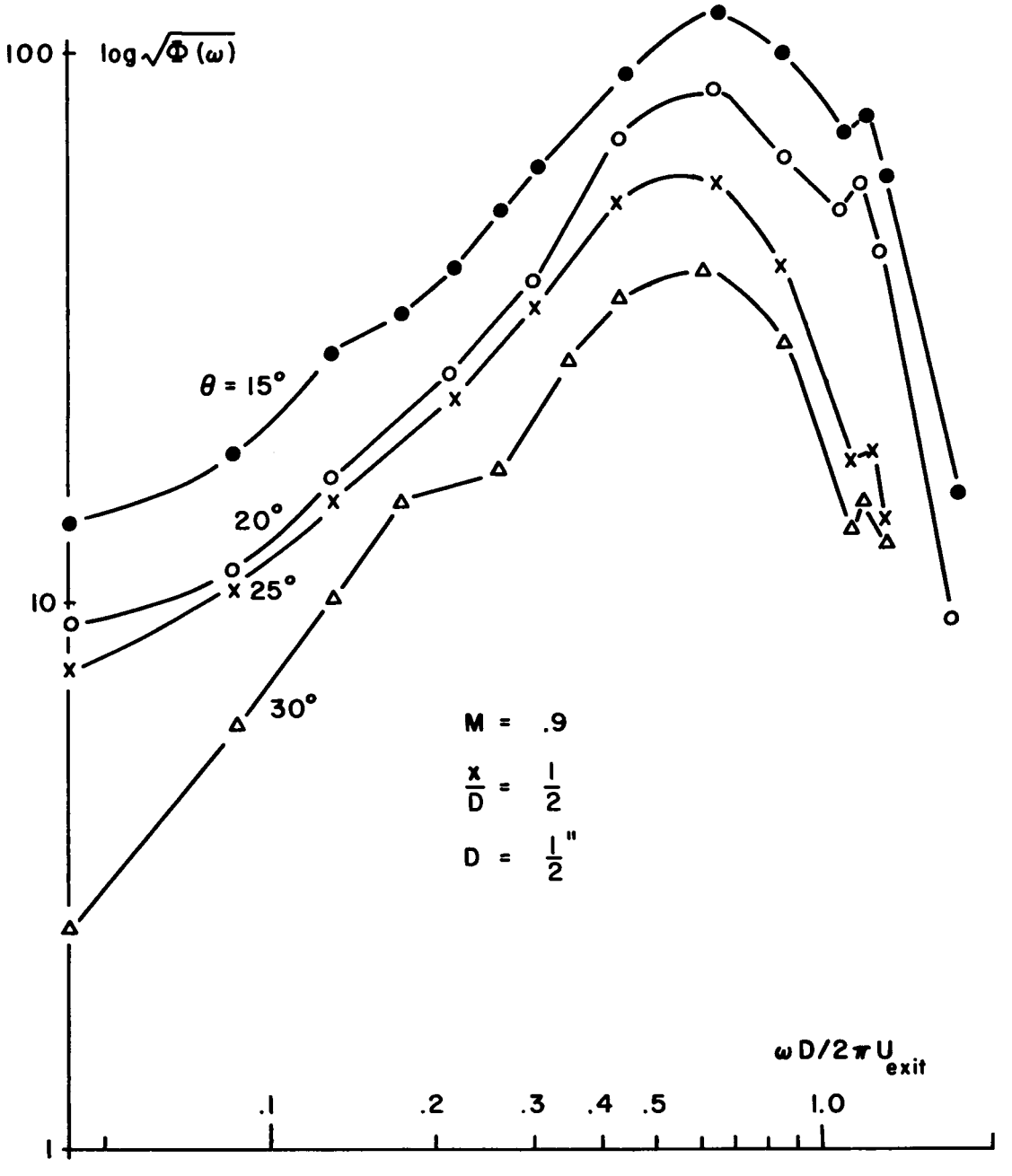

Figure 15. Near Field Spectra, x/D = 1/2
M_{exit} = 0.9, D = 1/2 in.

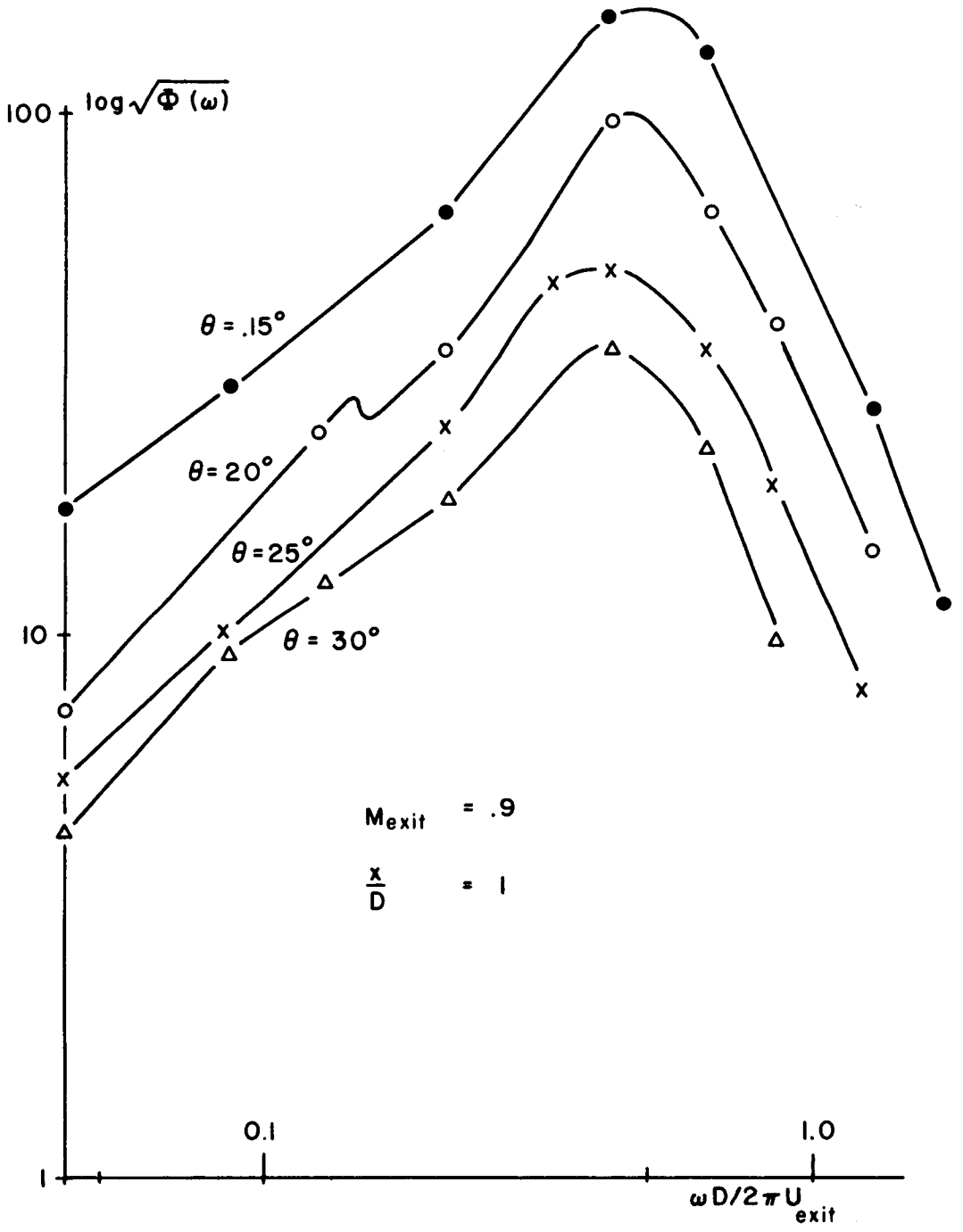

Figure 16. Near Field Spectra, x/D = 1
M_{exit} = 0.9, D = 1/2 in.

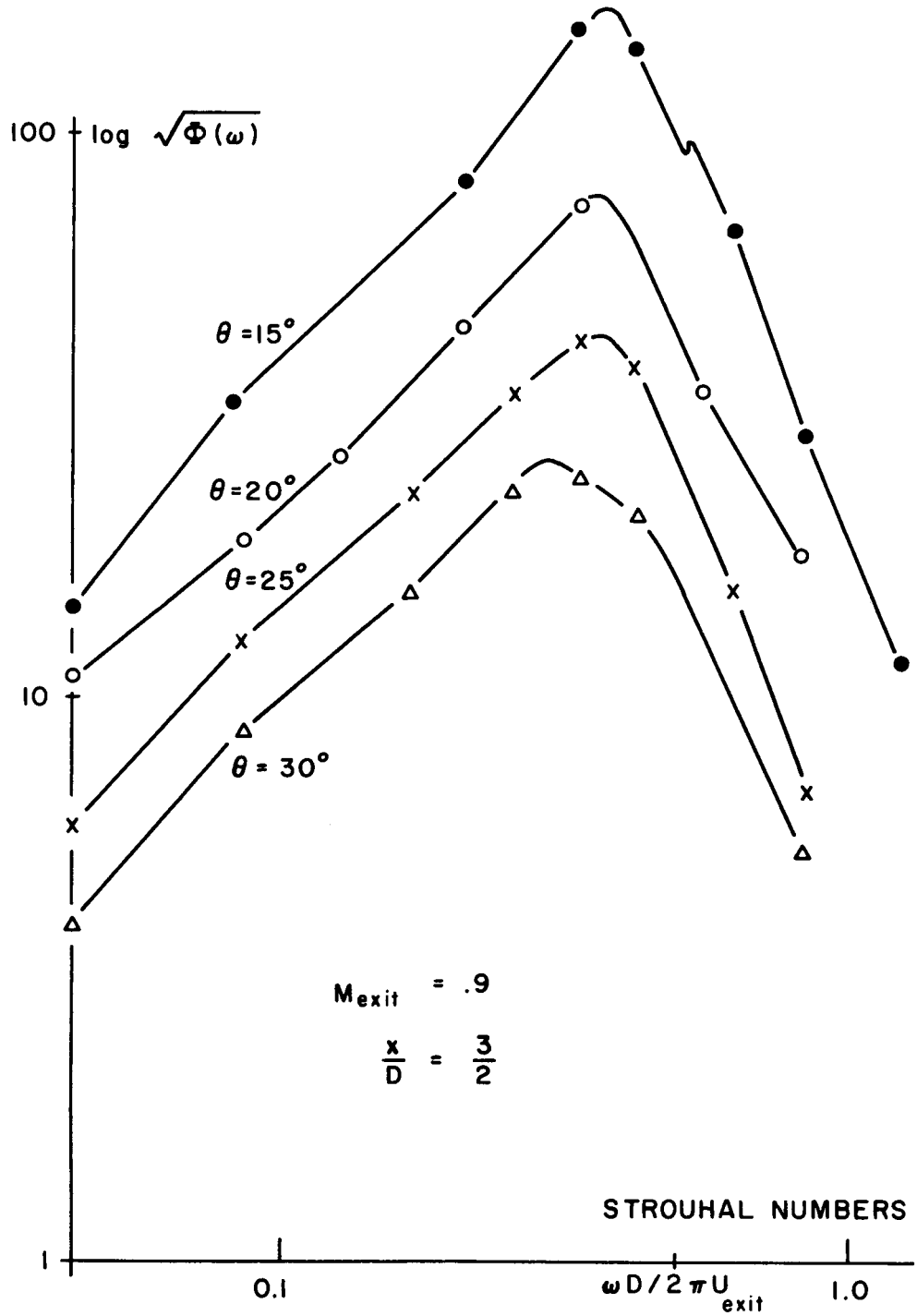

Figure 17. Near Field Spectra, x/D = 3/2
M_{exit} = 0.9, D = 1/2 in.

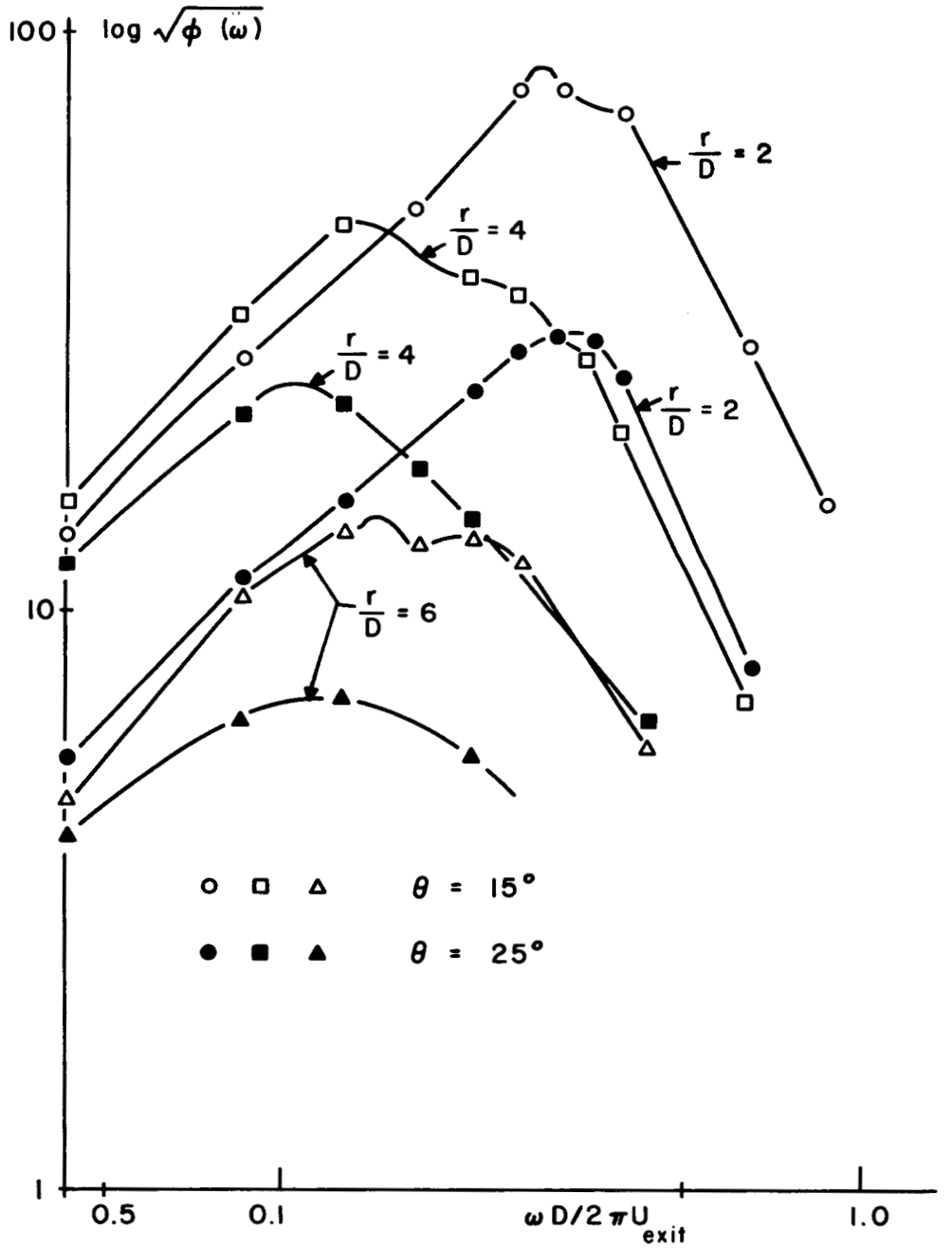

Figure 18. Spectra of Near Field Pressure M_{exit} = 0.9, D = 1/2 in.

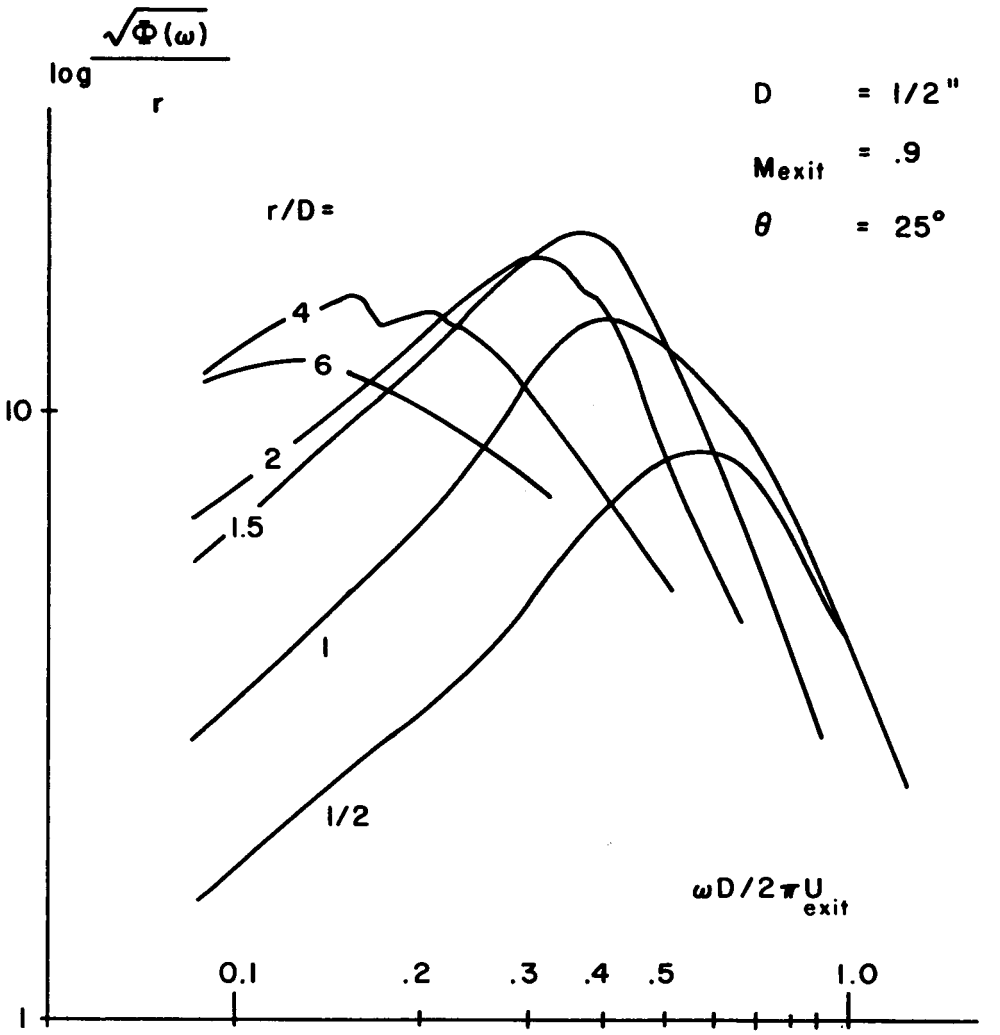

Figure 19. Near Field Spectra Showing Approach to Far Field Similarity of the Higher Frequencies.

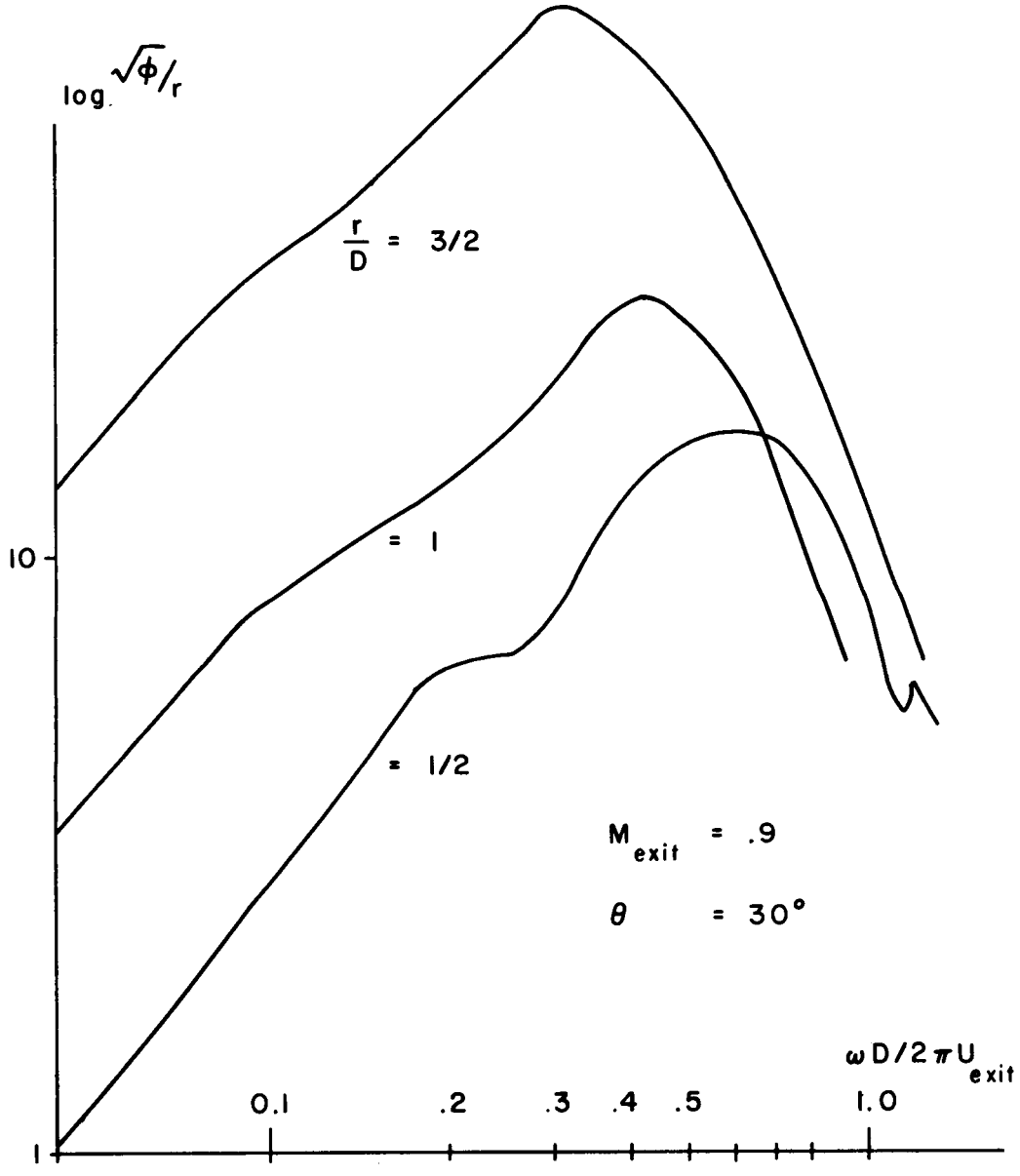

Figure 20. Near Field Spectral Similarity, Showing Approach to Far Field for High Frequencies

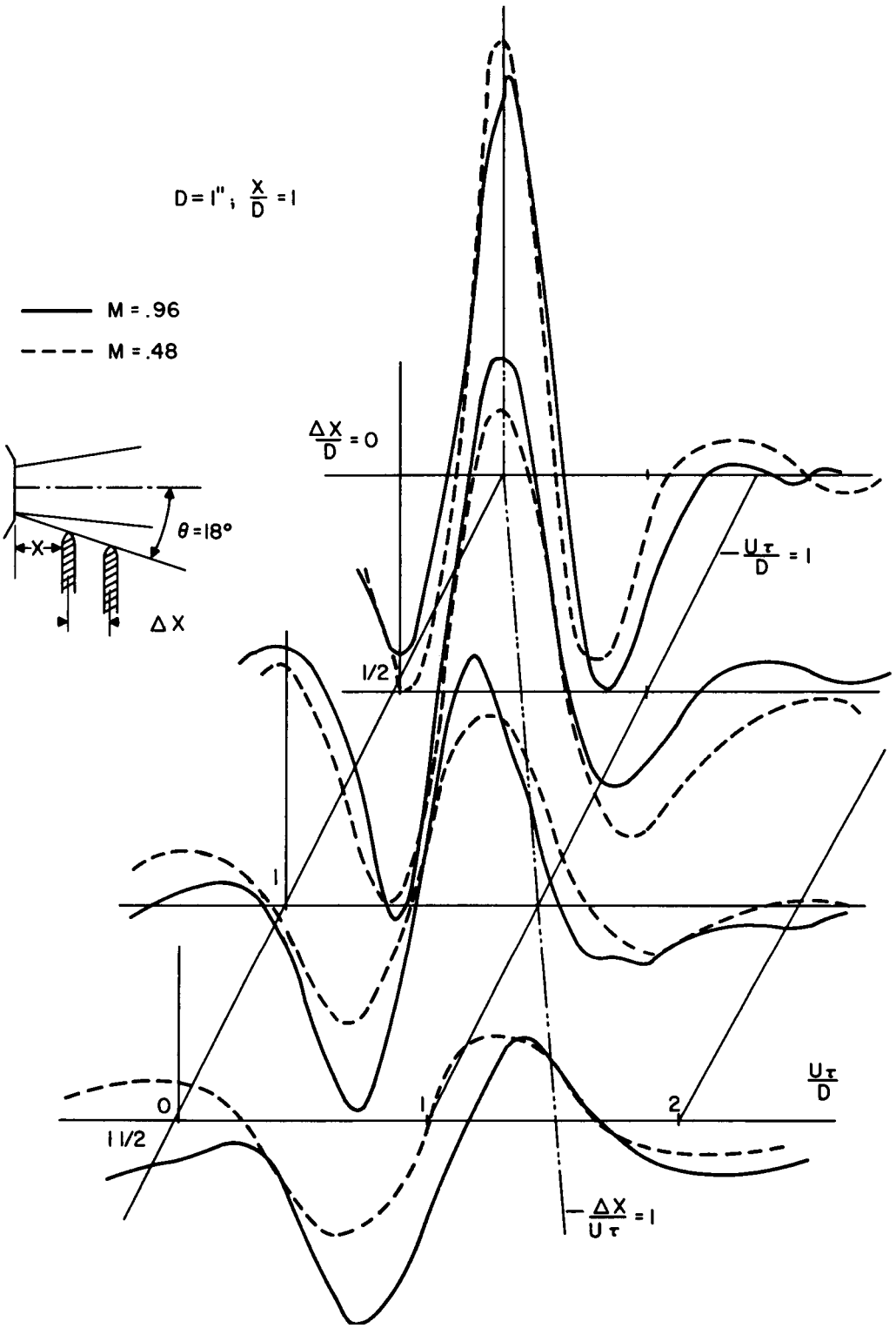

Figure 21. Similarity of Pressure Correlation Coefficient

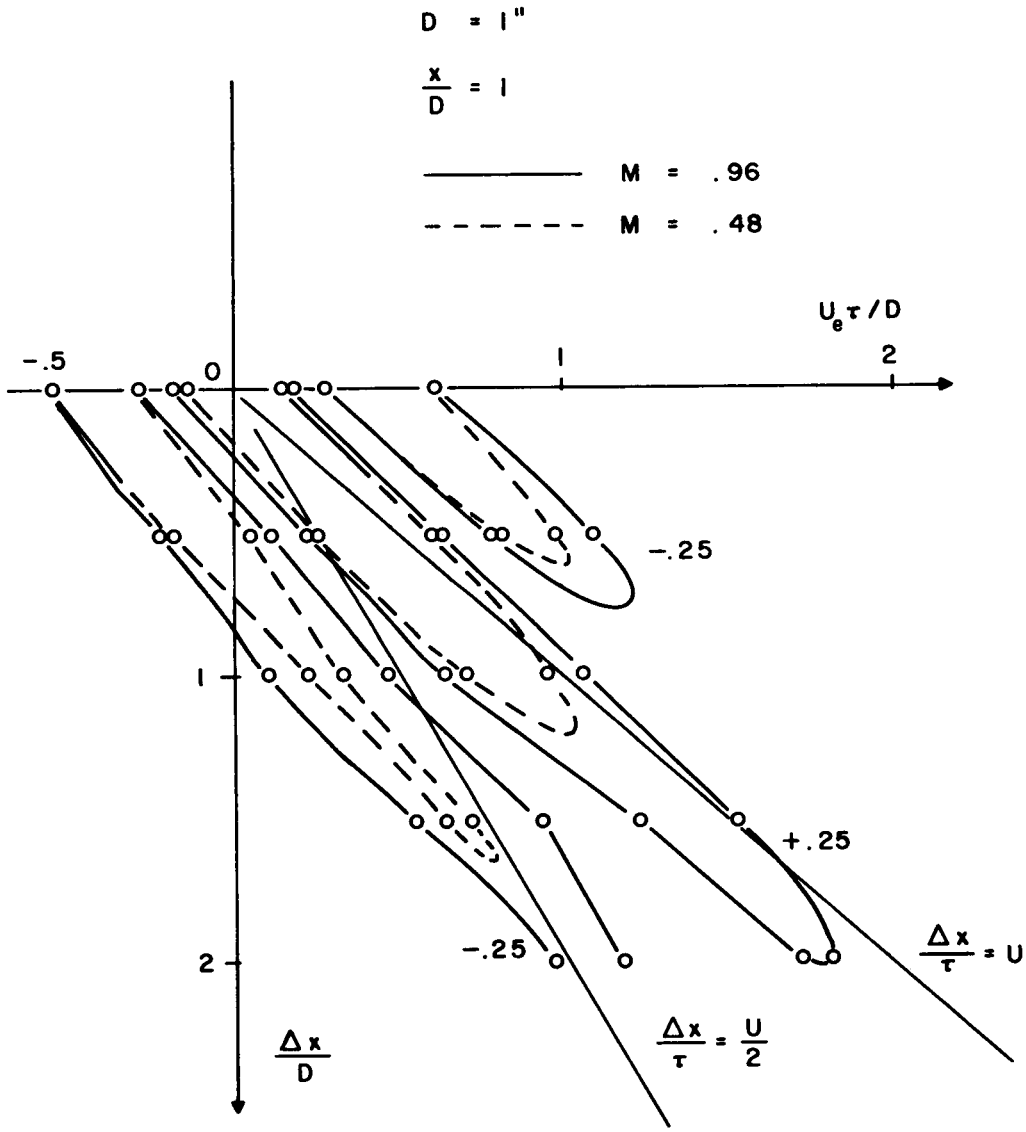

Figure 22. Contours of Constant Pressure Space-Time Correlation Coefficient along $\theta = 180^{\circ}$, D = 1 in., M = 0.48 and 0.96

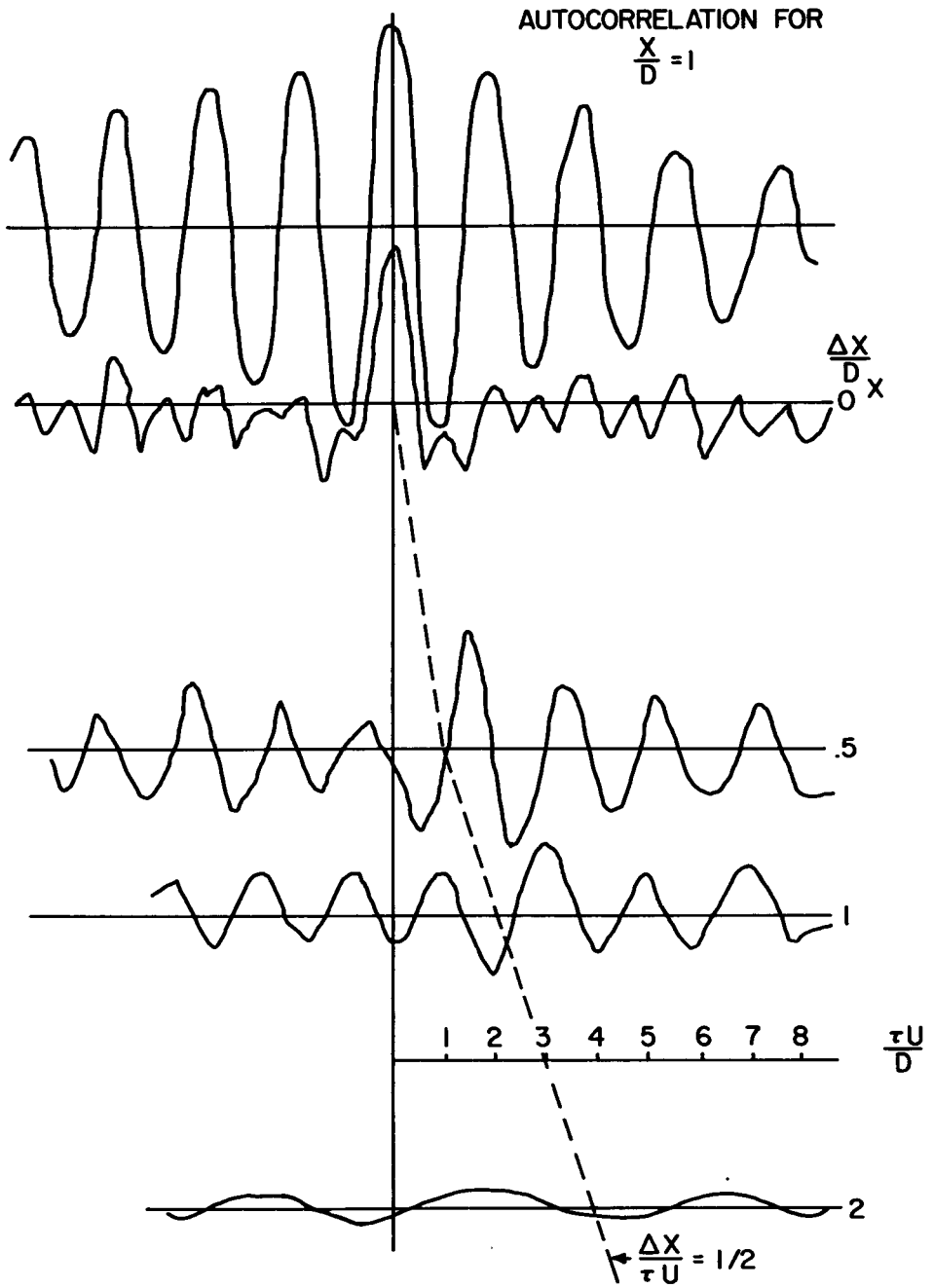

Figure 23. Pressure Space-Time Correlation Coefficient
M = 0.15; D = 1/2 in.; x/D = 1/2, θ = 15°

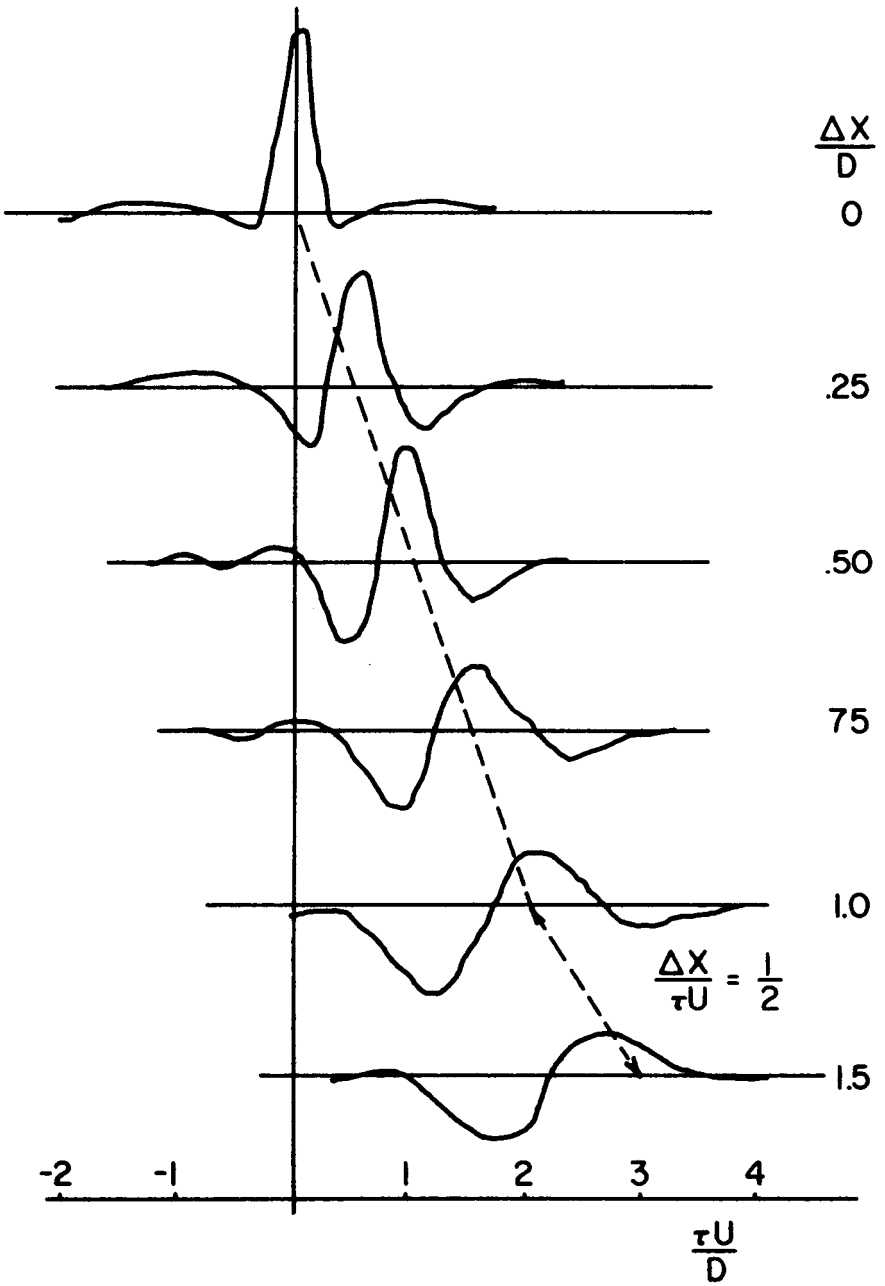

Figure 24. Pressure Space-Time Correlation Coefficient, M = 0.30; D = 1 in., x/D = 1/4; θ = 15°

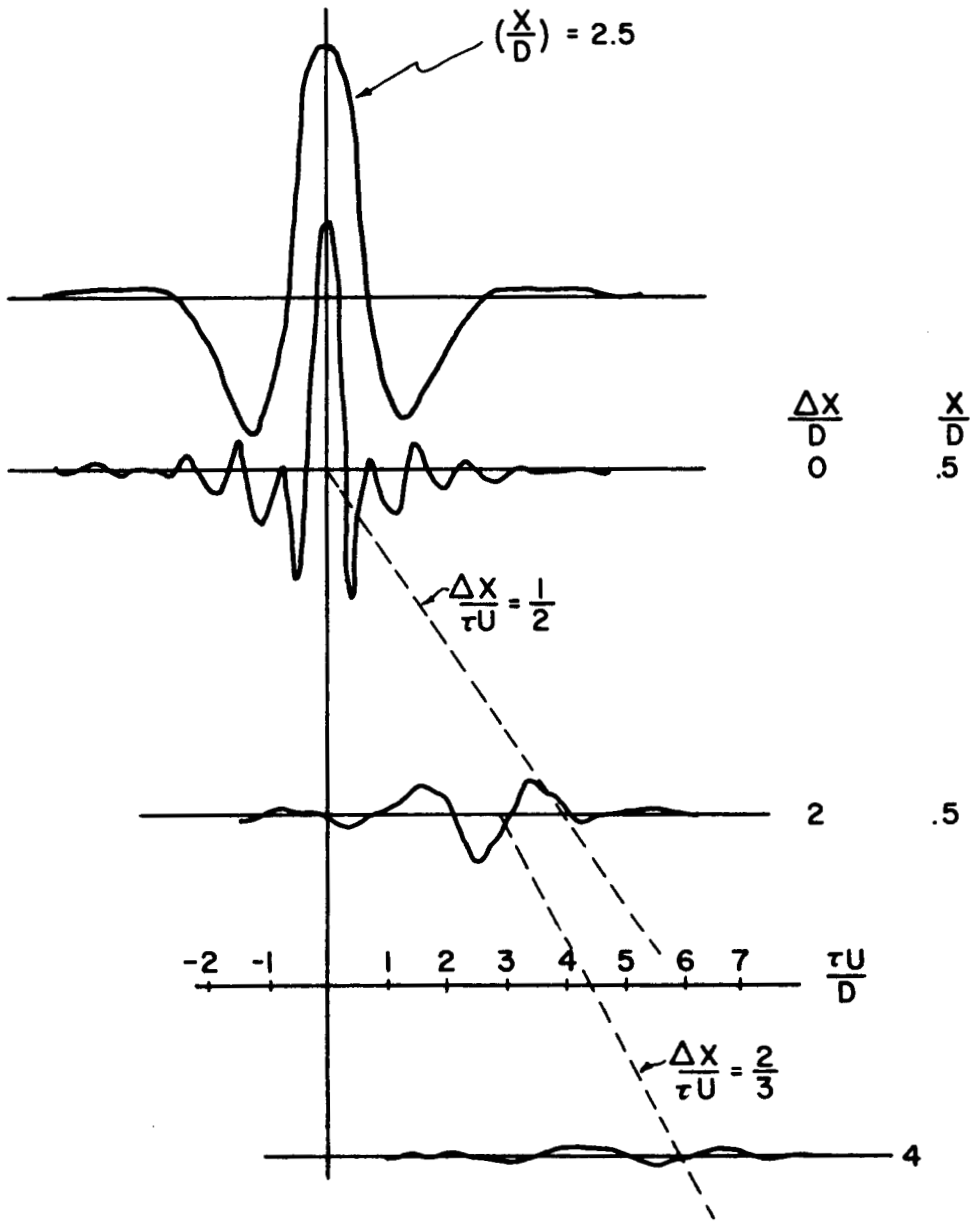

Figure 25. Pressure Space-Time Correlation Coefficient, M = 0.30; D = 1/2 in.; x/D = 1/2; θ = 15°

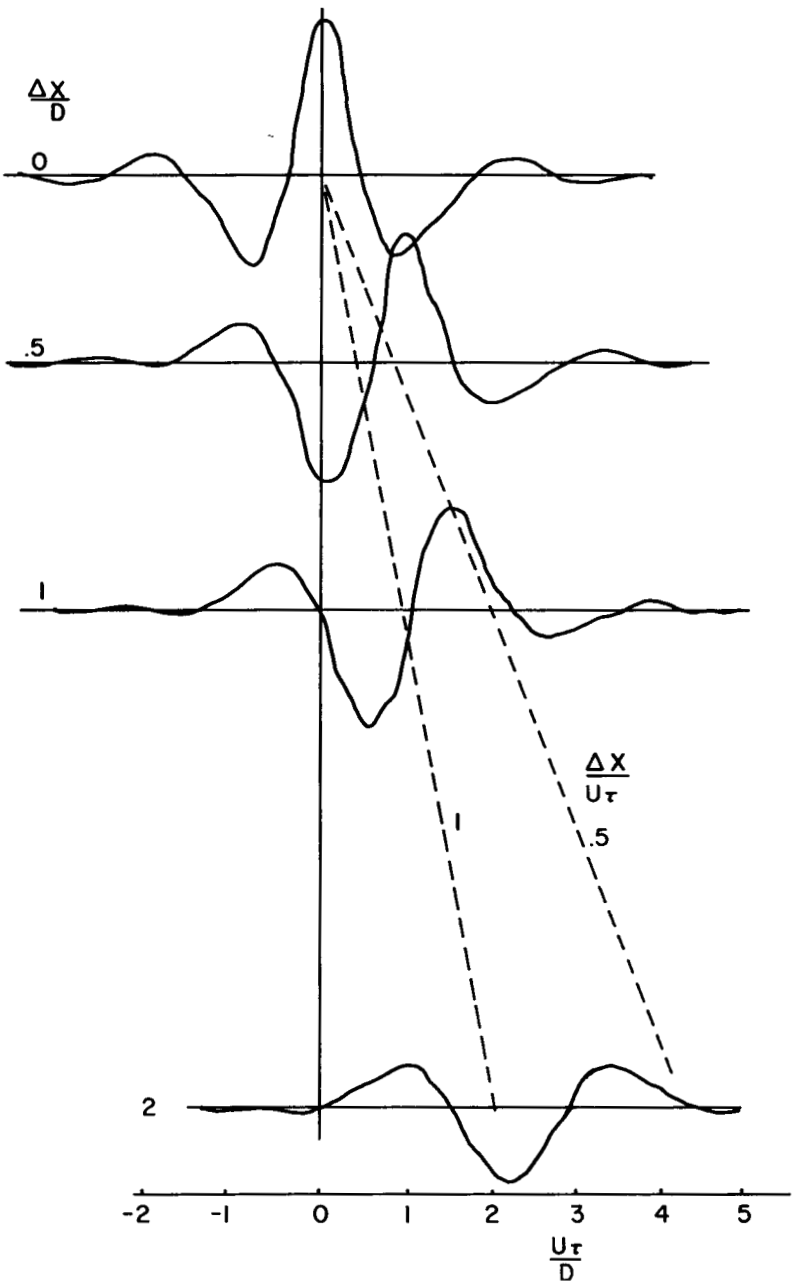

Figure 26. Pressure Space-Time Correlation Coefficient, M = 0.30; D = 1 in.; x/D = 1; $\theta = 18^{\circ}$

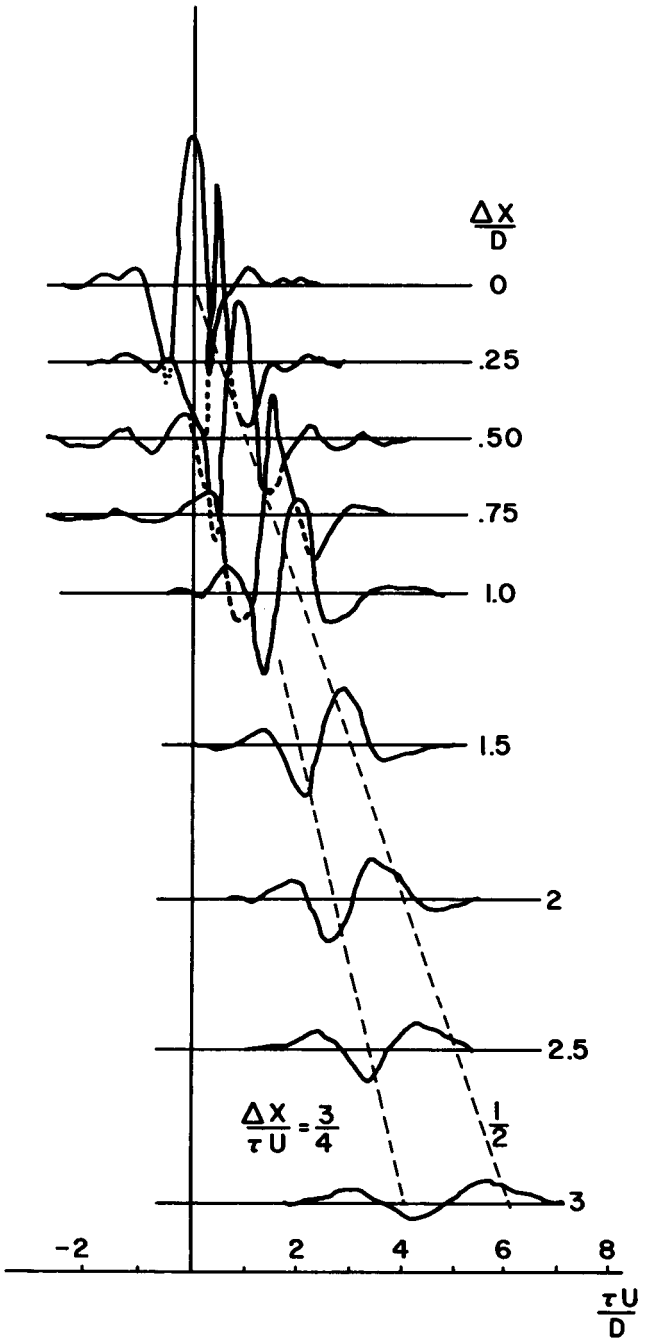

Figure 27. Pressure Space-Time Correlation Coefficient, M = 0.6; D = 1 in.; x/D = 1/4; $\theta = 15^{o}$

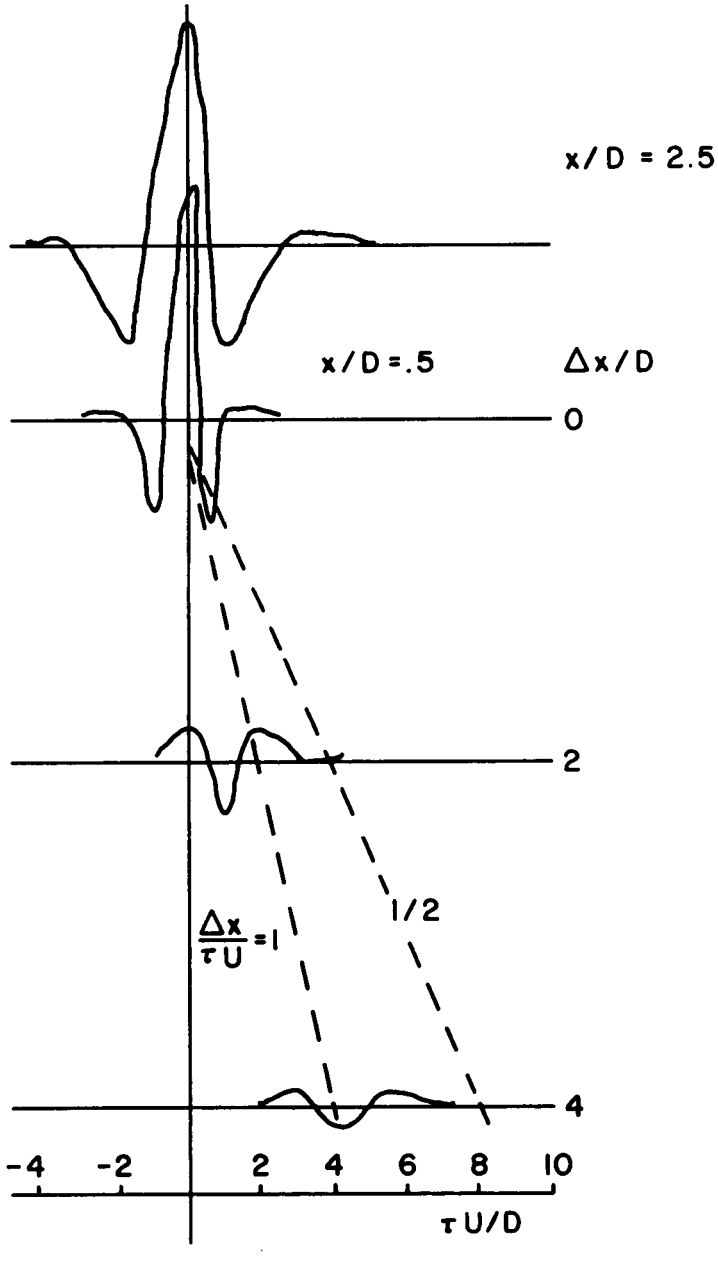

Figure 28. Pressure Space-Time Correlation Coefficient, M = 0.6; D = 1/2 in.; x/D = 1/2, θ = 15°

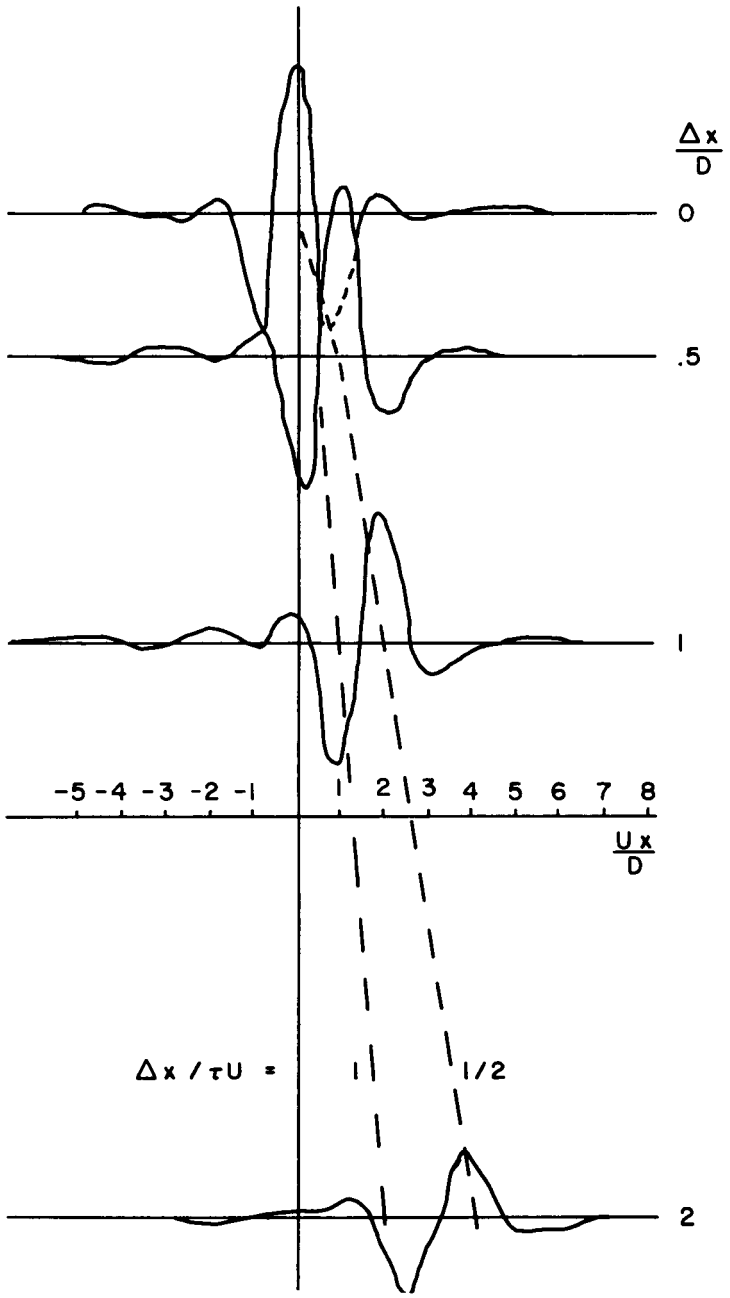

Figure 29. Pressure Space-Time Correlation Coefficient, M = 0.60; D = 1 in.; x/D = 1; θ = 18°

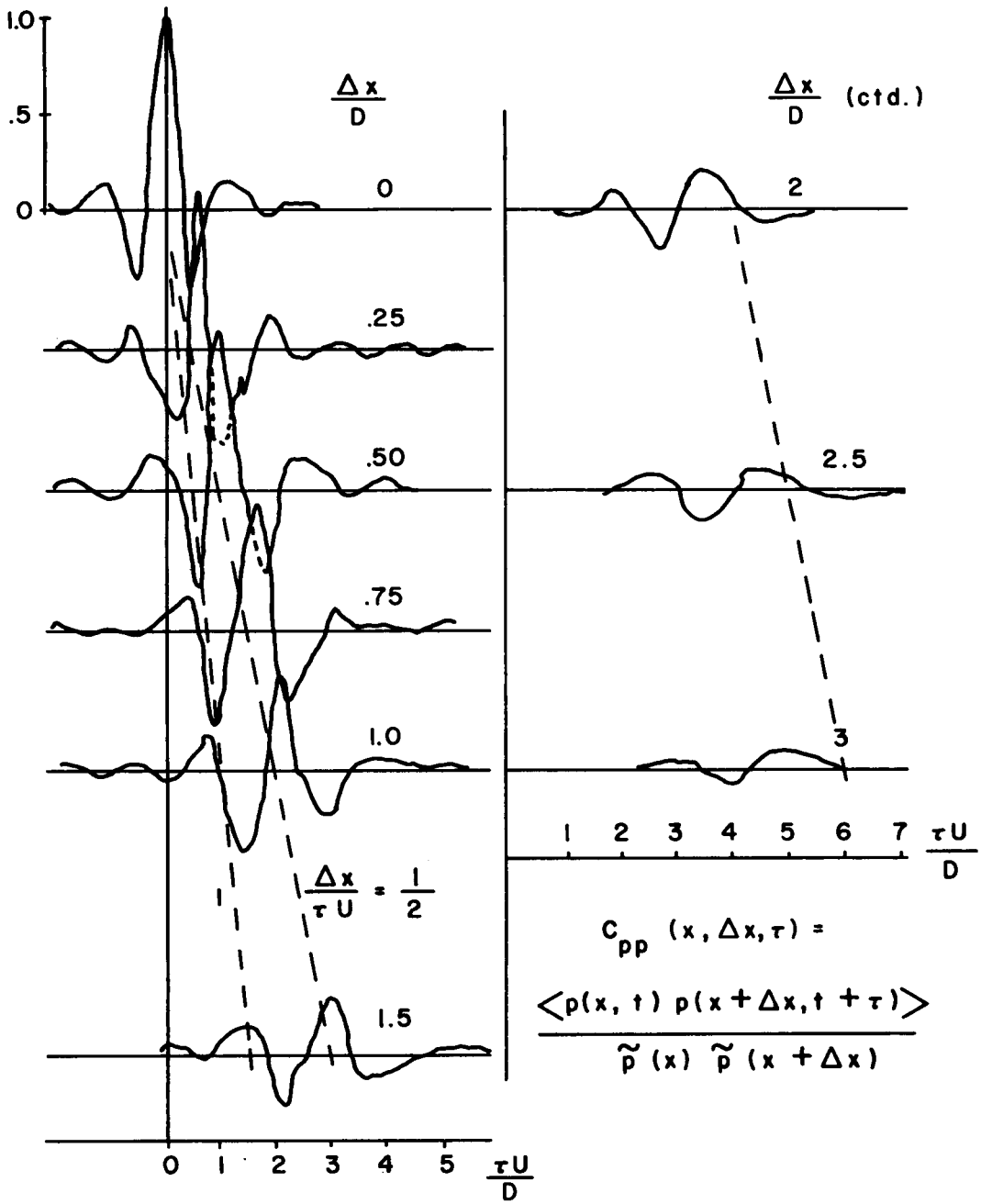

Figure 30. Pressure Space-Time Correlation Coefficient, M = 0.8; D = 1 in.; x/D = 1/4; $\theta = 15^{o}$

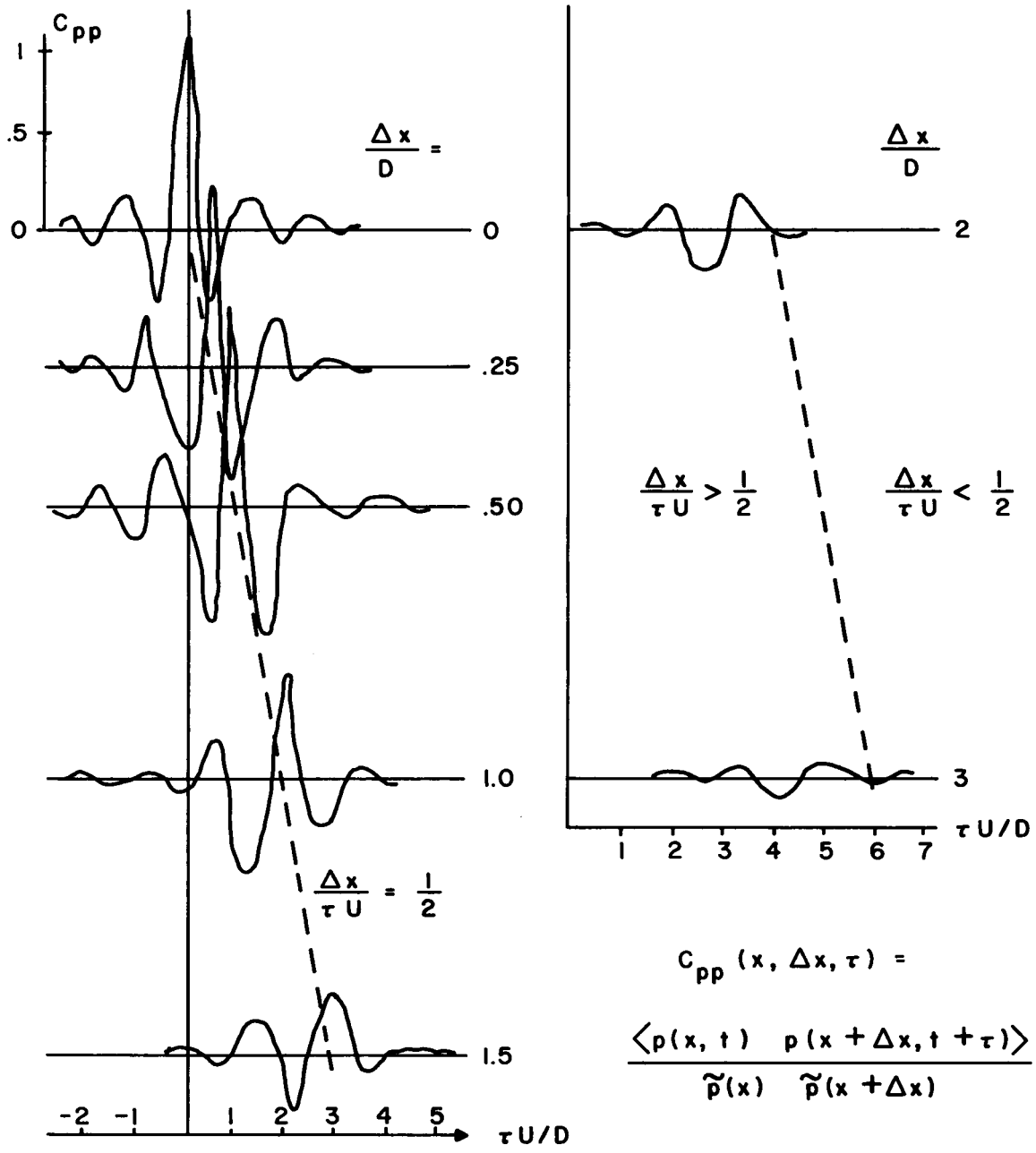

Figure 31. Pressure Space-Time Correlation Coefficient, M = 0.90, D = 1 in., x/D = 1/4; $\theta = 15^{o}$

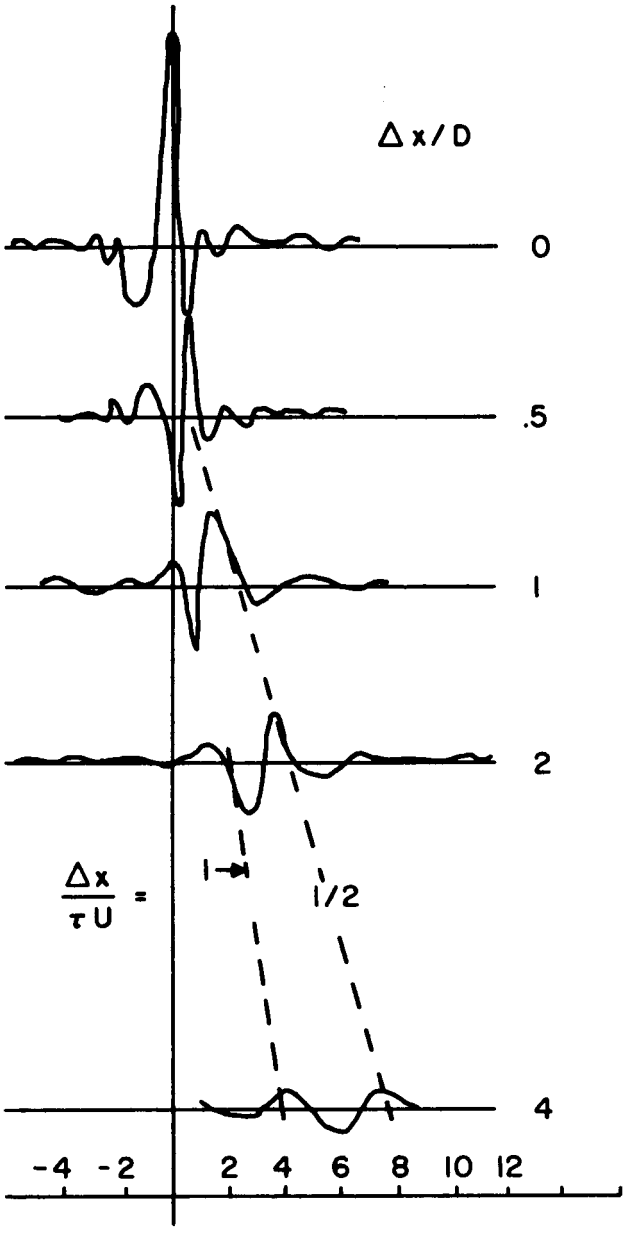

Figure 32. Pressure Space-Time Correlation Coefficient, M = 90; D = 1/2 in.; x/D = 1/2; θ 15°

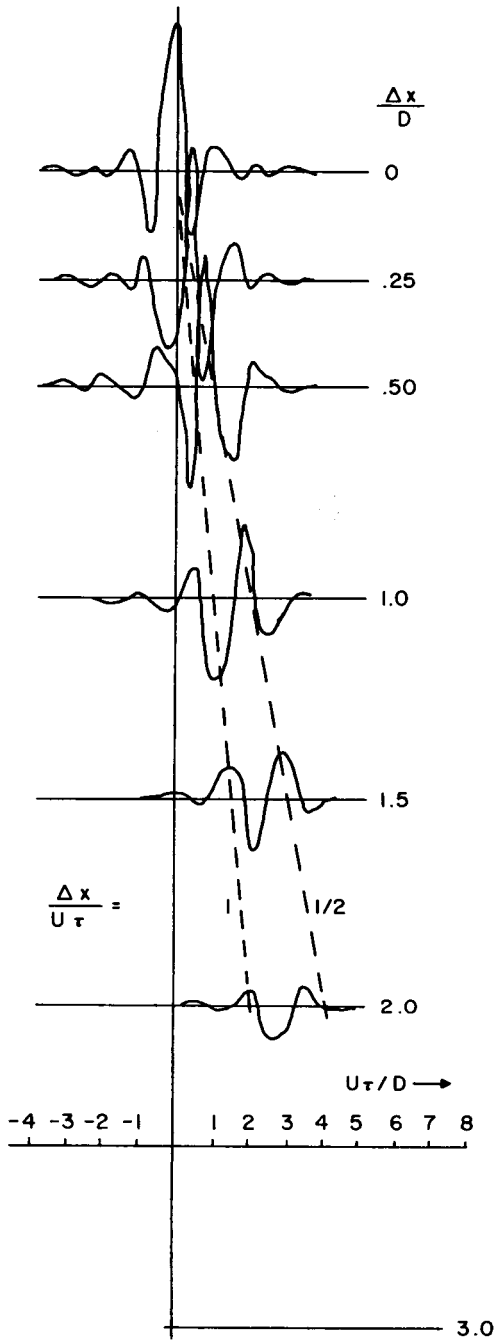

Figure 33. Pressure Space-Time Correlation Coefficient, M = 0.95; D = 1 in.; x/D = 1/4; θ = 20°

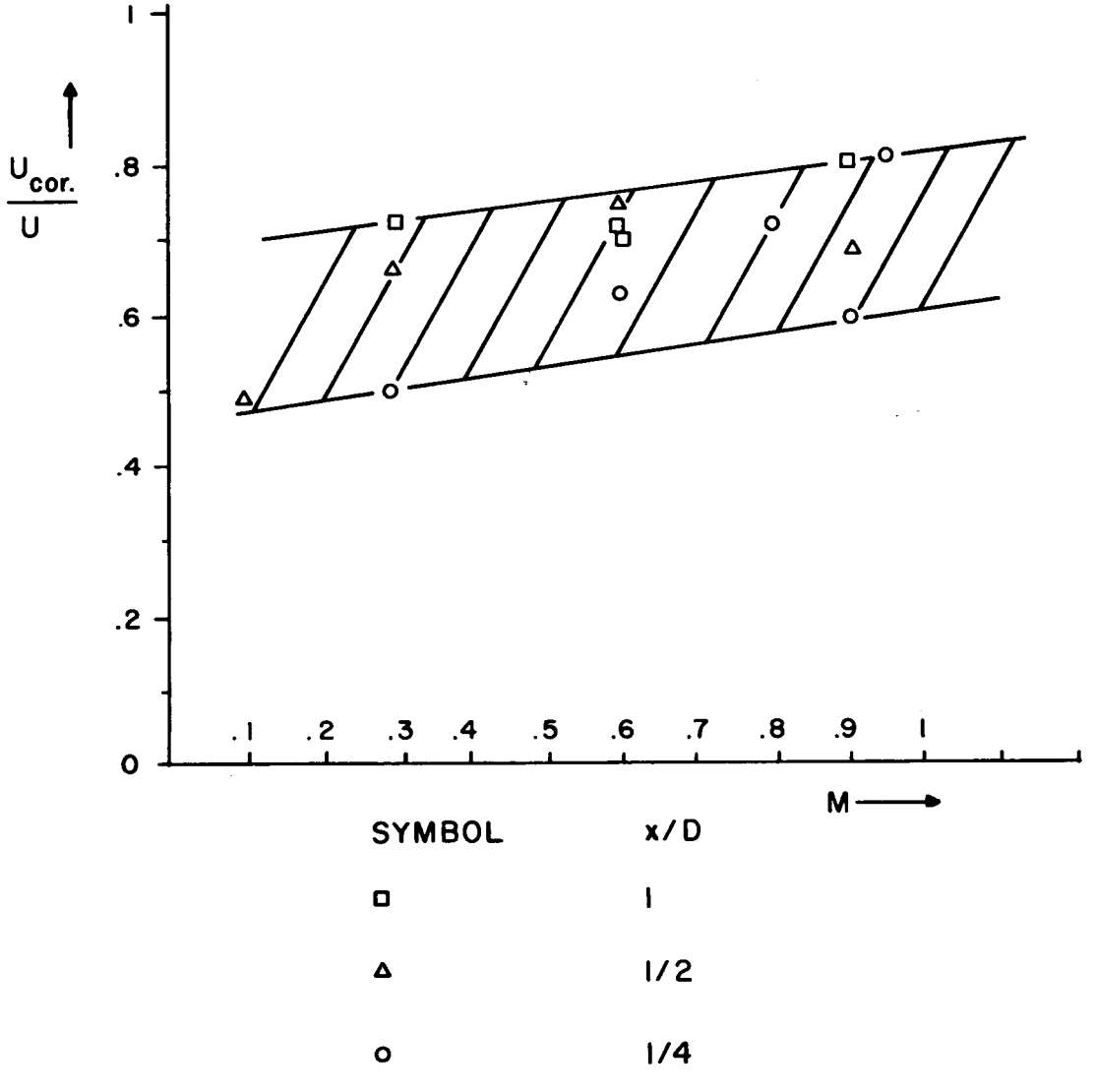

Figure 34. Observed Correlation Velocities

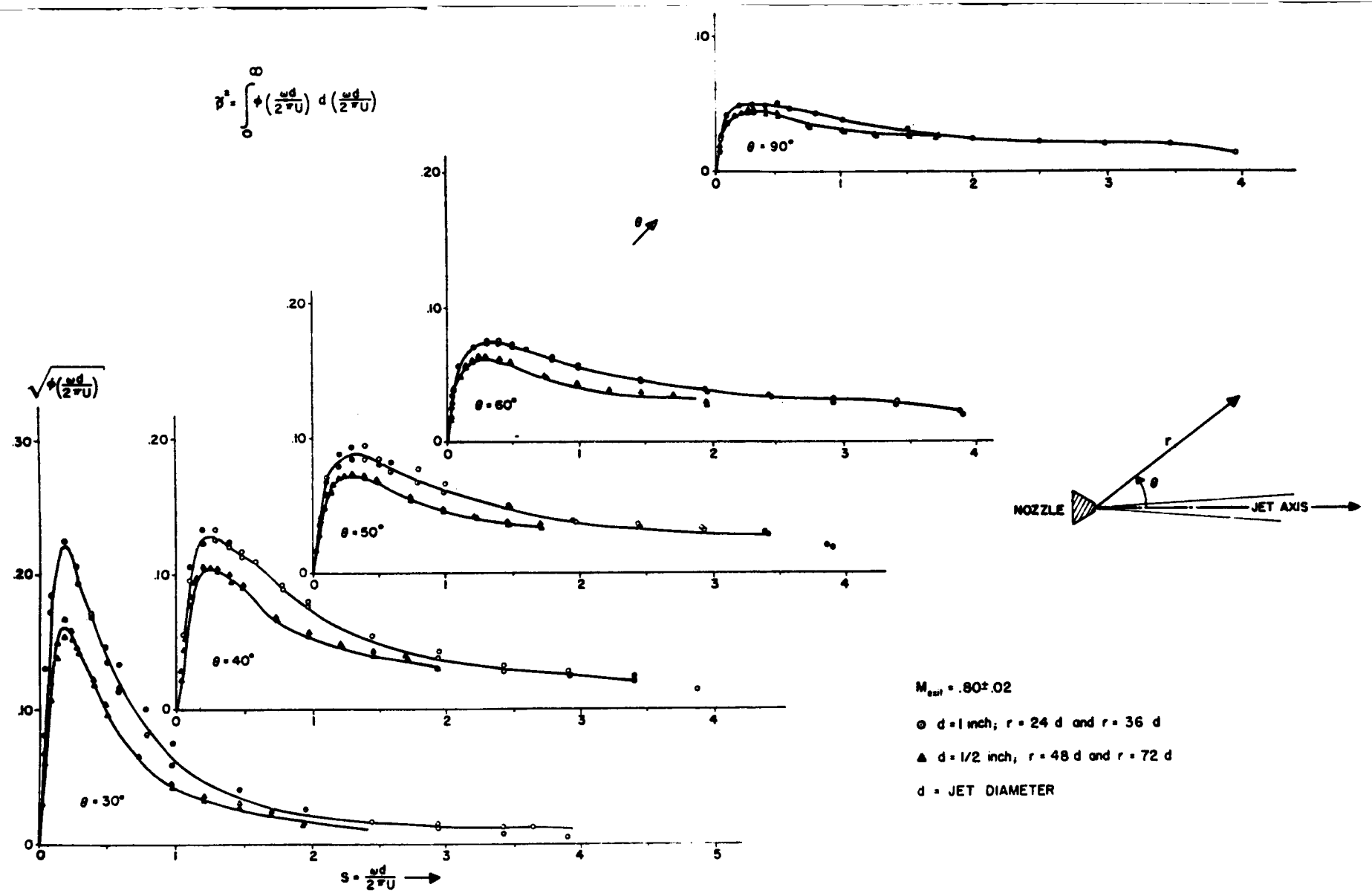

Figure 35. Far Field Spectra of Sound, $M_{exit} = 0.8$